Received: 31 March 2021 | Accepted: 8 November 2021

DOI: 10.1002/tpg2.20182

The Plant Genome

ORIGINAL RESEARCH

Integration of metabolomics and transcriptomics data to further characterize *Gliricidia sepium* (Jacq.) Kunth under high salinity stress

Thalliton Luiz Carvalho da Silva[1] | **Vivianny Nayse Belo Silva**[1] | **Ítalo de Oliveira Braga**[1] | **Jorge Candido Rodrigues Neto**[2] | **André Pereira Leão**[4] | **José Antônio de Aquino Ribeiro**[4] | **Leonardo Fonseca Valadares**[4] | **Patrícia Verardi Abdelnur**[2,4] | **Carlos Antônio Ferreira de Sousa**[3] | **Manoel Teixeira Souza Jr.**[1,4]

[1] Graduate Program of Plant Biotechnology, Federal Univ. of Lavras, 37200-000, Lavras, MG CP 3037, Brazil

[2] Institute of Chemistry, Federal Univ. of Goiás, Campus Samambaia, Goiânia, GO 74690-900, Brazil

[3] Brazilian Agricultural Research Corporation, Embrapa Mid-North, Teresina, PI 64008–780, Brazil

[4] Brazilian Agricultural Research Corporation, Embrapa Agroenergy, Brasília, DF 70770-901, Brazil

Correspondence
Manoel Teixeira Souza, Jr., Brazilian Agricultural Research Corporation, Embrapa Agroenergy, Brasília, DF, 70770-901, Brazil.
Email: manoel.souza@embrapa.br

Assigned to Associate Editor Lin Li.

Abstract

Soil salinity is one abiotic stress that threatens agriculture in more than 100 countries. Gliricidia [*Gliricidia sepium* (Jacq.) Kunth] is a multipurpose tree known for its ability to adapt to a wide range of soils; however, its tolerance limits and responses to salt stress are not yet well understood. In this study, after characterizing the morphophysiological responses of young gliricidia plants to salinity stress, leaf metabolic and transcription profiles were generated and submitted to single and integrated analyses. RNA from leaf samples were subjected to RNA sequencing using an Illumina HiSeq platform and the paired-end strategy. Polar and lipidic fractions from leaf samples were extracted and analyzed on an ultra-high-performance liquid chromatography (UHPLC) coupled with electrospray ionization quadrupole time-of-flight high-resolution mass spectrometry (MS) system. Acquired data were analyzed using the OmicsBox, XCMS Online, MetaboAnalyst, and Omics Fusion platforms. The substrate salinization protocol used allowed the identification of two distinct responses to salt stress: tolerance and adaptation. Single analysis on transcriptome and metabolome data sets led to a group of 5,672 transcripts and 107 metabolites differentially expressed in gliricidia leaves under salt stress. The phenylpropanoid biosynthesis was the most affected pathway, with 15 metabolites and three genes differentially expressed. Results showed that the differentially expressed metabolites and genes from this pathway affect mainly short-term salt stress (STS). The single analysis of the transcriptome identified 12 genes coding for proteins that might play a

Abbreviations: AE, age effect; AT, all treatments; DAT, days after treatment; DEP, differentially expressed peak; EC, electrical conductivity; FC, fold change; FDR, false discovery rate; LTS, long-term salt stress; *m/z*, mass-to-charge ratio; ROS, reactive oxygen species; RT, reference transcriptome; STS, short-term salt stress; UHPLC–MS/MS, ultra-high performance liquid chromatography–tandem mass-spectrometry.

role in gliricidia response at both STS and long-term salt stress (LTS). Further studies are needed to reveal the mechanisms behind the adaptation response.

1 | INTRODUCTION

The world population is on track to reach between 9 and 10 billion persons by 2050, resulting from an increase of more than 3 billion individuals in the first half of the 21st century. This scenario has challenged the biomass production system to produce more food, feed, fiber, bioenergy, and ornamentals, among other bioproducts derived from plants, in a sustainable way. The increase in biomass production must occur while plants are affected by several more intense abiotic and biotic stresses resulting from changes in climatic conditions (FAO, 2011). Soil salinity is one of the abiotic stresses that threaten agriculture the most, and it is a problem present in more than 100 countries spread across all continents. Approximately 20% of all agricultural land in the world has either saline or sodic soils, and between 25 and 30% of the irrigated land area is affected by salt (Shahid et al., 2018). From an agricultural point of view, saline soils contain sufficient neutral soluble salts that negatively affect the growth of most cultivated plants. A priori, those soils that present electrical conductivity of the soil saturation extract >4 dS m^{-1} at 25 ˚C are considered saline. However, since many fruits, vegetable, and ornamental species suffer from the adverse effects of salinity in a range of 2 to 4 dS m^{-1}, soils with an electrical conductivity (EC) in this range are then classified as saline when cultivating these kinds of plant species (Bresler et al., 1982; Vargas et al., 2018).

Gliricidia [*Gliricidia sepium* (Jacq.) Kunth], a medium-sized legume (10–15 m) that belongs to the Fabaceae family, is originated from Central America. It shows rapid growth and is one of the most well-known multipurpose trees. It is a crop cultivated for improving soil fertility, for medicinal purposes, for use as wood and firewood, as charcoal, and as a shade of plantations (Rahman et al., 2019). At the economic level, the gliricidia role in improving water infiltration and increasing water retention capability of the soil, reducing soil erosion, and restoring and improving the soil quality, leading to a higher crop yield, is highlighted (Diouf et al., 2017). It is also known for its ability to adapt to several soils including eroded acidic soils, sandy soils, heavy clay, limestone, and alkaline soils (Rahman et al., 2019).

Gliricidia salinity tolerance limits, alongside its responses to salt stress, are not yet well understood (Rahman et al., 2019). Rahman and colleagues showed that seawater-induced salinity negatively affected several growth-related attributes in 1-mo-old gliricidia seedlings and then postulated that proline, which showed enhanced accumulation under salinity stress, might help gliricidia plants to adjust to water deficit conditions. Proline participates in metabolic signaling and is known to be metabolized by its own family of enzymes responding to stress (Phang et al., 2010).

There are many transcriptomics and metabolomics studies on plants' responses to stress (Cavill et al., 2016; Jamil et al., 2020). Transcriptomics is a technology applied to characterize the transcriptome in a cell, tissue, or organism at any given time. Unlike the genome that tends to be static information, the transcriptome is variable; and is one of the links between the genome and the phenotype of an organism (Wang et al., 2009; Zhang et al., 2010). Metabolomics is a technology applied to characterize the complete set of small-molecule chemicals found within a biological sample. Metabolites are functional products of metabolism, and their concentration levels vary according to genetic or physiological changes. Since it provides a better representation of an organism's phenotype than any other omic, metabolomics emerges as an efficient tool to fill the phenotype-genotype gap (Zampieri & Sauer, 2017).

Because of the rise in accessibility to high-throughput biological data from different omics, efforts to analyze these data separately have given rise to a more comprehensive view and with a focus on integrating different omics to obtain more robust knowledge of biological systems (Cavill et al., 2016; Jamil et al., 2020). The first successful integrative attempts using these two omics in fungi and plants date almost two decades (Askenazi et al., 2003; Urbanczyk-Wochniak et al., 2003; Hoefgen & Nikiforova, 2008). Since then, many groups have used distinct integrative approaches to gain insights into many different plant traits. Transcript and metabolite are not directly associated; however, the process of integrating them provides information that allows us to base the phenotypic data and measures provided by the metabolomics on the genetic data from the transcriptome (Cavill et al., 2016; Jamil et al., 2020). Yan and colleagues identified new target genes and metabolites by integrating data from these two omics in *Tetrastigma hemsleyanum* Diels et Gilg, showing that these molecules led to a gain of efficiency of the anthocyanin metabolic pathway (Yan et al., 2020). Rai et al. (2020) also did it to identify genes involved in the biosynthetic pathways of the dominant groups of bioactive metabolites in *Cornus officinalis* Siebold & Zucc., an important medicinal plant.

In this study, we first carried out a morphophysiological characterization of the response of gliricidia to salinity stress in both the short- and long-term and at five different doses of NaCl. We then produced the metabolome and transcrip-

tome profiles from the leaves and applied single-omics analysis and integration pathway-based strategies to characterize the metabolome and transcriptome data.

Core Ideas

- This study shows the morphophysiological responses of gliricidia to high salinity stress.
- This study evaluates the tolerance and the adaptation responses of gliricidia to high salinity stress.
- This study uses single and integrated analyses of gliricidia metabolome and transcriptome under high salinity stress.
- The role of the phenylpropanoid biosynthesis pathway in gliricidia response to high salinity stress is explored.

2 | MATERIALS AND METHODS

2.1 | Plant material and growth conditions

The accession of gliricidia used in this study belongs to the Gliricidia Collection at Embrapa Tabuleiros Costeiros (www.embrapa.br/en/tabuleiros-costeiros). After soaking the seeds in 2% sodium hypochlorite and Tween 20 for 5 min under slow agitation, we washed them with sterile water and dried them on sterilized filter paper. Then they were placed in a Petri dish with filter paper moistened with sterilized water until the radicle emission. Subsequently, seedlings were transferred individually to a 5-L plastic pot containing 4 kg of substrate previously prepared by mixing sterile soil, vermiculite, and a commercial substrate (Bioplant) in the ratio 2:1:1 (v:v:v) and kept in a greenhouse for 3 mo.

2.2 | Experimental design and saline stress

Three-month-old gliricidia plants were subjected to saline stress (0.0, 0.4, 0.6, 0.8, and 1.0 g of NaCl per 100 g of substrate) for 2 d (short-term salt stress [STS]) or 45 d (long-term stress salt [LTS]). The experimental design was completely randomized with five replicates (plants) per treatment.

The NaCl was dissolved in deionized water to salinize the substrate. The amount of deionized water used corresponded to the difference between the amount previously present in the substrate and the amount necessary for the substrate to reach field capacity. Applying the right amount of water—up to the substrate field capacity—was a means of ensuring no leakage of the solution out of the pot and no loss of Na^+ or Cl^-. The moisture content, the field capacity, and the EC of the substrate at field capacity were measured by applying the same protocols described for oil palm (*Elaeis guineensis* Jacq.) by Vieira et al. (2020).

The water lost because of evapotranspiration was replaced daily with deionized water, and EC and the water potential in the substrate solution measured at 0, 6, 35, and 45 d after treatment (DAT) to impose the salt stress for all replicates.

2.3 | Biomass and mineral analysis

Plant biomass was determined by harvesting the gliricidia plants at the end of the experiment, separating them into their parts, that is, canopy and roots, and weighing them for fresh biomass determination. After being dried in a forced-air oven at 65 ˚C to constant weight to determine dry biomass, the samples were ground in a Wiley mill Tecnal Mod. TE 680 (Tecnal), passed through a 1-mm (20 mesh) sieve and then subjected to extraction of minerals by the standard methods used in laboratory routine at Soloquímica (www.soloquimica.com.br). The data from the mineral analysis was initially analyzed using bidirectional analysis of variance (ANOVA). To compare the treatments with significant differences, we used the Tukey test ($p < .05$).

2.4 | Metabolomics analysis

After collecting the leaves for metabolomics analysis from all replicates at 2 and 45 DAT, we immediately immersed them in liquid nitrogen and stored them at −80 ˚C until extraction of metabolites. Samples were ground in liquid nitrogen before solvent extraction. The solvents methanol grade UHPLC, acetonitrile grade LC-MS, formic acid grade LC-MS, and sodium hydroxide ACS grade LC-MS were from Sigma-Aldrich, and the water treated in a Milli-Q system (Millipore).

We employed a protocol adapted from the Max Planck Institute (Rodrigues-Neto et al., 2018; Vargas et al., 2016), known as 'all-in-one' extraction, to extract the metabolites. After transferring aliquots of 50 mg of ground sample to 2-ml microtubes, 1 ml of 1:3 (v:v) methanol/methyl tert-butyl ether at −20 ˚C was added and then left for homogenization on an orbital shaker at 4.0 ˚C for 10 min followed by an ultrasound treatment in an ice bath for another 10 min. Next, added 500 µl of 1:3 (v:v) methanol/water mixture to each microtube before centrifugation (15,300 x *g* at 4.0 ˚C for 5 min). After centrifugation, three phases were generated: an upper nonpolar (green), a lower polar (brown), and a remaining protein pellet. The nonpolar and polar fractions were transferred separately to 1.5-ml microtubes and vacuum dried in a Speed vac (Centrivap, Labconco).

2.4.1 | UHPLC–MS and UHPLC–MS/MS

After resuspending the dry polar fraction by adding 500 µl of 1:3 (v:v) methanol: water mixture, it was transferred to a vial and analyzed by ultra-high performance liquid chromatography–tandem mass-spectrometry (UHPLC–MS/MS). We used a UHPLC chromatographic system (Nexera X2, Shimadzu Corporation) equipped with an Acquity UPLC HSS T3 (1.8 µm, 2.1 by 150 mm) reverse phase column (Waters Technologies), maintained at 35 ˚C. Solvent A was 0.1% (v/v) formic acid in water and solvent B was 0.1% (v/v) formic acid in acetonitrile/methanol (70:30, v/v). The gradient elution used, with a flow rate of 0.4 ml min^{-1}, was as follows: isocratic from 0 to 1 min (0% B), linear gradient from 1 to 3 min (5% B), from 3 to 10 min (50% B), and 10 to 13 min (100% B), isocratic from 13 to 15 min (100% B), followed by rebalancing in the initial conditions for 5 min. The rate of acquisition spectra was 3.00 Hz, monitoring a mass range from mass-to-charge ratio (*m/z*) 70–1200 (polar fraction) and *m/z* 300–1600 (lipidic fraction).

Detection was performed by high-resolution mass spectrometry (MaXis 4G Q-TOF MS, Bruker Daltonics GmbH & Co.) using electrospray source in positive (electrospray ionization(+)-MS) and negative (electrospray ionization(−)-MS). The settings of the mass spectrometer were as follows: final plate offset, 500 V; capillary voltage, 3800 V; nebulizer pressure, 4 bar; dry gas flow, 9 L min^{-1}; and dry temperature, 200 ˚C. The rate of acquisition spectra was 3.00 Hz, monitoring a mass range of *m/z* 70 to 1200. A sodium formate solution (10 mM HCOONa solution in 50:50 v/v isopropanol/water containing 0.2% formic acid) was injected directly through a six-way valve at the beginning of each chromatographic run for external calibration. Ampicillin ([M + H] + *m/z* 350.11867 and [M − H] − *m/z* 348.10288) was added to each sample and used as an internal standard for peak normalization.

Tandem mass spectrometry parameters were adjusted to improve mass fragmentation with collision energy ranging from 20 to 50 eV using a step method. Precursor ions were acquired using the 3.0 s cycle time. The general AutoMS settings were as follows: mass range, *m/z* 70–1000 (polar fraction) and *m/z* 300–1600 (lipidic fraction); spectrum rate, 3 Hz; ionic, positive polarity; pre-pulse storage, 8 µs; funnel 1 RF, 250.0 Vpp. The UHPLC–MS and UHPLC–MS/MS data were acquired by HyStar Application v3.2 (Bruker Daltonics GmbH & Co.).

2.4.2 | Metabolomics data analysis

The raw data from UHPLC–MS were exported as mzMXL files using DataAnalysis 4.2 software (Bruker Daltonics) and preprocessed using XCMS Online (Gowda et al., 2014; Tautenhahn et al., 2012) for peak detection, retention time correction, and alignment of the metabolites detected in the UHPLC–MS analysis. Peak detection was performed using centWave peak detection ($\Delta m/z$ = 10 ppm; minimum peak width, 5 s; maximum peak width, 20 s) and mzwid = 0.015, minfrac = 0.5, bw = 5 for alignment of retention time. The unpaired parametric *t* test (Welch *t* test) was used for statistical analysis.

The processed data (CSV file) were exported to MetaboAnalyst 4.0 and submitted to the Statistical Analysis module (Chong & Xia, 2020; Chong et al., 2019). Before the chemometric analysis, all data variables from the polar fraction were normalized by internal standard (ampicillin-rT = 7.9 min; [M + H], *m/z* 350.11711, [M − H], *m/z* 348.10212) and all data variables from the lipidic fraction were normalized by internal standard (1,2-diheptadecanoyl-sn-glycero-3-phosphocholine = 4.85 min; [M + H], *m/z* 762.60063). All sets of data were scaled using the Pareto method.

The differentially expressed peaks (DEPs) were selected according to the following criteria: variable importance in projection (VIP) values ≥ 0.99 obtained from the partial least squares discriminant analysis model; adjusted *P* value (false discovery rate [FDR]) ≤ 0.05 of the Welch *t* test; and Log_2 (fold change [FC]) ≠ 1. The selected DEPs were then submitted to analysis in the mass spectrometry Peaks to Pathway module (Chong & Xia, 2020; Chong et al., 2019) using molecular weight tolerance of 5 ppm, mixed ion mode, joint analysis using the mummichog algorithm (Li et al., 2013) with a *P* value cutoff of 1.0×10^{-5}, the Gene Set Enrichment Analysis (Subramanian et al., 2005) algorithms, and the latest KEGG version of the *Arabidopsis thaliana* pathway library.

In the case of a DEP with two or more matched forms (isotopes) and later a matched compound with two or more DEPs, the initial criterion of metabolite selection applied was the mass difference compared with the metabolite database, choosing the smallest one. The second criterion was the adduct study of each candidate back in its mass spectra. Then, we applied the formula and exact mass data from KEGG. Finally, we performed the putative annotation of the metabolites of interest with one or two candidates on each detected ion.

The KEGG IDs of the matched compounds were then submitted to pathway analysis (integrating enrichment analysis and pathway topology analysis) and visualization in the Pathway Analysis module (Chong & Xia, 2020; Chong et al., 2019) and analyzed using the hypergeometric test and the latest KEGG version of the *A. thaliana* pathway library.

2.5 | Transcriptomics analysis

Leaves for transcriptomics analysis, collected from all replicates at 2 and 45 DAT, were immediately immersed in liquid nitrogen and stored at −80 ˚C until RNA extraction. The

Qiagen RNeasy Plant Mini kit was used for total RNA extraction following the manufacturer's protocol. RNA quantity was measured using a Nanodrop Qubit 2.0 Fluorometer (Life Technologies) and RNA quality with an Agilent Bioanalyzer Model 2100 (Agilent Technologies). RNA sequencing using an Illumina HiSeq platform was done at the GenOne Company (www.genone.com.br) using the paired-end strategy.

2.5.1 | Transcriptomics data analysis

The transcriptomics analyses were all done on OmicsBox v1.3 (BioBam, 2019). We used FastQC (Andrews, 2010) and Trimmomatic (Bolger et al., 2014) to perform the quality control, filter reads, and to remove low-quality bases. The minimum average quality of reads kept was 30, and the minimum length of reads was 75. The reference transcriptome used was generated using the following software: Trinity v2.8.5 (Grabherr et al., 2011) and Bowtie2 v2.3.5.1 (Langmead & Salzberg, 2012). The RNA sequencing data were aligned to the reference transcriptome using default parameters from OmicsBox v1.3 through software STAR v2.7.8a (Dobin et al., 2013) and to quantify expression at the level of gene or transcript, we used the default parameters from OmicsBox v1.3 through HTSeq v0.9.0 (Anders et al., 2015).

The pairwise differential expression analysis between different experimental conditions was performed through edgeR v3.28.0 (Robinson et al., 2010), applying a simple design and an exact statistical test without using any filter for low-count genes. The normalization method used was 'trimmed mean of M' values. The statistical test used was the exact test (based on the quantile-adjusted conditional maximum likelihood methods [similar to Fisher's exact test]). To select the differentially expressed genes (DEGs), we applied the following criteria: adjusted P value (FDR) ≤ 0.05 and Log_2 (FC) $\neq 1$. To perform the functional analysis of the DEGs, we combined the differential expression results with functional annotations from the high-throughput functional annotation and data mining pipeline in OmicsBox v1.3 (Götz et al., 2008).

2.6 | Integratomics analysis

Omics Fusion (Brink et al., 2016), the web platform for integrative analysis of omics data (https://fusion.cebitec.uni-bielefeld.de), was employed for carrying out the integrative analysis of transcripts and metabolites. The input data used was the Log_2 (FC) data of the differentially expressed genes (FDR ≤ 0.05 and Log_2 (FC) $\neq 1$) and metabolites (VIP ≥ 0.99, FDR ≤ 0.05, and Log_2 (FC) $\neq 1$) obtained from the single-omics analysis in OmicsBox v1.3 (BioBam, 2019) and MetaboAnalyst 4.0 (Chong & Xia, 2020; Chong et al., 2019), respectively. First, to check the data distribution, we used the Data Overview module and then the scatter plot one for the correlation analysis between the two sets of data, a pairwise combination of the different scenarios evaluated.

For subsequent analysis, we used the modules KEGG feature distribution and map data on the KEGG pathway. The former module was employed to verify which metabolic pathways had more transcripts and metabolites differentially expressed and the latter to map these data differentially expressed in the metabolic paths in question. For the KEGG feature distribution module, we applied the joint analysis of transcripts and metabolites with a threshold of 10 and for the map data on the KEGG pathways using the organism code gmx (Glycine max) for mapping.

3 | RESULTS

3.1 | Gliricidia response to salt stress

The addition of increasing levels of NaCl to the substrate led to an increase in EC and a reduction in water potential as expected (Figure 1a and 1b). The saline level of 0.0 g of NaCl, which did not receive the addition of NaCl, unexpectedly presented an EC of ~7.5 dS m^{-1}, putting this treatment in the range of saline stress. As is shown in the soil analysis, it is not due to an ionic effect of the salts present in the chemical fertilizers added to the substrate (Supplemental Table S1).

The amount of water used to measure EC in this study was enough for the substrate to reach the field capacity (maximum amount of water it can hold) and not enough to saturate the substrate. So, the EC measured was not the EC of the saturated extract but rather the EC of the substrate at field capacity. The EC of the substrate at field capacity is higher than the EC of the saturated extract, as the salts in this former are in less water than in the latter. Because of this, this treatment was then not considered a no-salt stress control; instead, it is a low salinity stress treatment. Consequently, all salt treatments used in this study provided EC higher than that of a soil considered as saline, or >4.0 dS m^{-1}.

Both canopy (Figure 1c) and roots (Figure 1d) dry biomass decreased directly proportional to the increase of NaCl in the substrate. Regarding canopy and roots dry biomass at 45 DAT, the root/canopy ratio increased as the NaCl dose increased in the substrate up to 0.8 g.

The doses of salt in the substrate and the weather and climatic conditions influenced the evapotranspiration rates. The evapotranspiration rate values showed a negative correlation to the NaCl dose applied to the plant substrate. Thus, the saline level that showed the highest value of real evapotranspiration rate was the treatment with 0.0 g of NaCl. As the saline levels increased, it led to a proportional reduction in the actual evapotranspiration rate. However, at 45 DAT, the evapotranspiration rate in all saline levels was practically similar (data not shown).

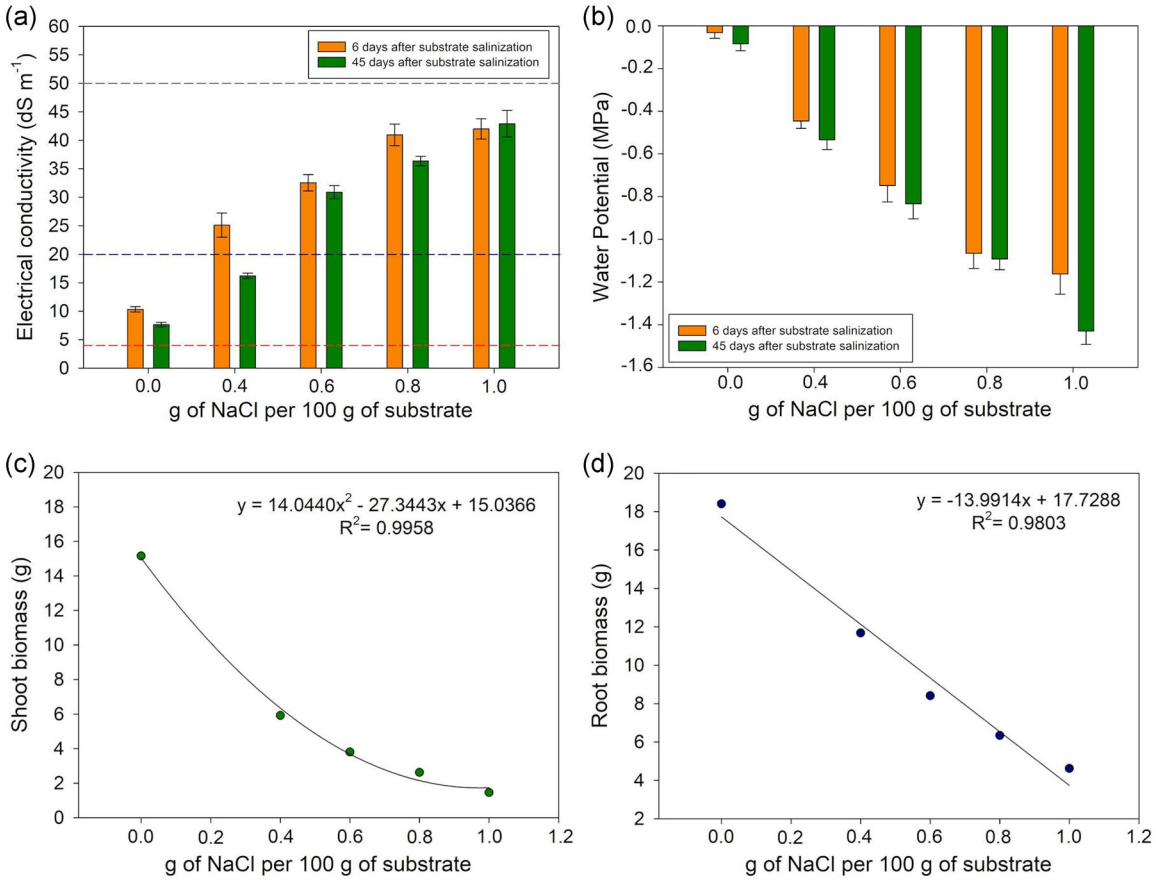

FIGURE 1 (a) Electrical conductivity (EC) and (b) water potential of the substrate used for growing gliricidia plants to which different levels of NaCl have been added at 6 and 45 d after substrate salinization. Red dashed line, EC = 4 dS m^{-1} (above that level is considered saline soil); blue dashed line, EC = 20 dS m^{-1} (plant completing its life cycle above this EC is considered as halophyte); and gray dashed line, EC = 50 dS m^{-1} (seawater salinity). Biomass accumulation in the (c) canopy and (d) roots of gliricidia plants grown under different concentrations of NaCl for 45 d. The values represent the average of five replicates, and the bars represent the standard error of the mean

The methodology established for the application and monitoring of salinity stress in gliricidia, employing a substrate salinization protocol, allowed the identification of two distinct responses of these gliricidia plants to salt stress depending on the amount of NaCl used. First, plants grown for 45 d on a substrate with 0.0 and 0.4 g of NaCl (approximately 7.5 and 15 dS m^{-1}, respectively) did not show any visual symptoms of stress on the aerial parts, such as leaf wilt, yellowing, burning, or falling, although they experienced a reduction in the canopy (Figure 1c) and root (Figure 1d) biomass. This type of response to salt stress was named tolerance.

On the third day after starting the salt stress, the leaves in plants submitted to ≥0.6 g of NaCl per 100 g of substrate showed a strong wilt symptom (Figure 2b), and in the fourth day, the leaves started to fall (Figure 2c). Some plants showed some burning in the leaves (Figure 2d). At the end of the first week of stress, plants at ≥30 dS m^{-1} lost almost all leaves (Figure 2e). However, ~3 wk after the beginning of the salt stress, it was possible to see some new leaves starting to emerge from the lateral meristems (Figure 2f), and their growth continued throughout the rest of the experiment (Figure 2g and 2h). This type of response to salt stress was named adaptation response.

As expected, the addition of increasing levels of NaCl led to an increase in the concentration of ions Na^+ and Cl^- in the substrate and a consequent one in the index of saturation by sodium as well (Supplemental Table S1). Gliricidia plants under salt stress accumulated more Na^+ in the canopy than in the roots. Indeed, most halophytes pile up more sodium in their leaves under salt stress (van Zelm et al., 2020). The amount of ion Cl^- in the canopy increase as the level of NaCl in the substrate increase, reaching a peak around 2.2 mg L^{-1} ppm.

The addition of NaCl also led to an increase in the availability of potassium in the soil solution. Approximately two-thirds of the accumulated K^+ in the plant was present in the canopy (Supplemental Table S1). Halophyte plants maintain a higher level of potassium than glycophytes and a more optimal K^+/Na^+; the cellular balance between sodium and potassium is a condition key for plant survival in saline soils (van Zelm

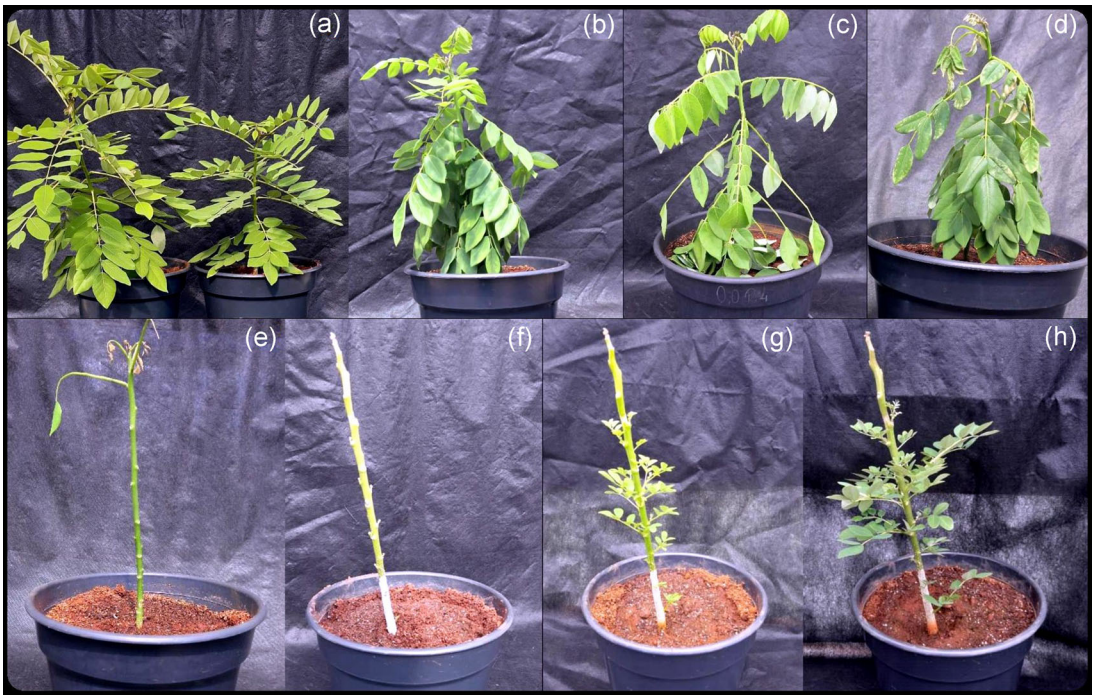

FIGURE 2 Symptoms of salt stress in gliricidia plants leaves. (a) Plants at 0.0 g of NaCl per 100 g of the substrate. (b) On the third day after starting the salt stress, the leaves from plants at 0.6 g of NaCl per 100 g of the substrate started to show a strong wilt symptom, and (c) in the fourth day after treatment (DAT) they started to fall. (d) Some plants presented 'burning' symptoms in some leaves. (e) At the end of the first week of stress, the stressed plants had lost almost all leaves, and (f) ~3 wk after the beginning of the stress, new leaves started to emerge, and (g, h) kept growing continuously throughout the rest of the experiment

et al., 2020). The K^+/Na^+ in the canopy and roots of gliricidia plants decreased directly proportional to the increase of NaCl in the substrate (Supplemental Table S1). The ion Ca^{2+} did not alter its availability in the solution because of the increasing level of NaCl added, and there was no significant difference in the amount of Ca^{2+} accumulated in the roots, independent of the NaCl dose applied. However, in the canopy, one can see a decrease in Ca^{2+} as the NaCl increases.

Plants respond to salt stress usually with a reduction in the assimilation of N (Ashraf et al., 2018). That was the case in both the canopy and the roots of gliricidia plants as the NaCl concentration increased in the substrate (Supplemental Table S1). Magnesium ion concentrations in the substrate and the plants do not change with the increase in NaCl levels. The amount of boron in the canopy significantly reduced as the levels of NaCl increased. Zinc in the substrate did not change because of the increase in NaCl levels, except for the highest concentration. The increasing levels of NaCl added did not significantly alter the zinc concentration in the canopy; however, in the roots, one can see a drop.

3.2 | Gliricidia metabolome under salinity stress

Based on the results of the morphophysiological characterization, we then selected the following treatments for metabolomics analysis: samples treated with 0.0, 0.4, 0.6, 0.8, and 1.0 g of NaCl, at 2 and 45 DAT with five replicates per treatment.

The following four data sets were employed to analyze the metabolome: all treatments (AT, all samples at 2 and 45 DAT); age effect (AE, samples treated with 0.0 g of NaCl at 2 and 45 DAT); STS (samples treated with 0.0 and 0.8 g of NaCl at 2 DAT); and LTS (samples treated with 0.8 g of NaCl at 2 and 45 DAT); all with five biological replicates.

The AT data set model was validated employing the partial least square discriminant analysis permutations test using a permutation number of 2,000. When evaluated by groupseparation distance, the probability of creating the model by chance was <0.0005% independent of the fraction—polar-positive, polar-negative, and lipidic-positive (Supplemental Figures S2A, S2C, and S2E). The evaluation by prediction accuracy showed that it was <0.0065% for the polar-positive and <0.0005% for the other two fractions (Supplemental Figures S2B, S2D, and S2F).

As already stated in the Materials and Methods section, a DEP is a peak with VIP value ≥ 0.99, FDR ≤ 0.05, and Log_2 (FC) > 1 (upregulated) or Log_2 (FC) < −1 (downregulated). Once it was clear that the number of DEPs was <10% in all scenarios tested (Table 1), a new question emerged: What would happen to the peaks differentially expressed in the STS scenario once the stressed plants reached the LTS scenario?

TABLE 1 Differentially expressed peaks and features in the leaves of gliricidia plants submitted to salinity stress in three distinct scenarios: age effect (AE, control plants at 2 and 45 d under salinity stress [DAT]); short-term stress (STS, control and the stress plants at 2 DAT); and long-term stress (LTS, stressed plants at 2 and 45 DAT)

Metabolomics	No. of peaks	Up	Down	Same
AE, control plants at 45 DAT vs. control plants at 2 DAT				
Polar-positive	1,368 (100%)	39 (2.85%)	135 (9.87%)	1,194 (87.28%)
Polar-negative	1,798 (100%)	3 (0.17%)	123 (6.84%)	1,672 (92.99%)
Lipidic-positive	4,190 (100%)	112 (2.67%)	256 (6.11%)	3,822 (91.22%)
STS, stressed plants at 2 DAT vs. control plants at 2 DAT				
Polar-positive	1,380 (100%)	93 (6.74%)	46 (3.33%)	1,241 (89.93%)
Polar-negative	1,817 (100%)	37 (2.04%)	29 (1.60%)	1,751 (96.37%)
Lipidic-positive	4,190 (100%)	127 (3.03%)	175 (4.18%)	3,888 (92.79%)
LTS, stressed plants at 45 DAT vs. stressed plants at 2 DAT				
Polar-positive	1,370 (100%)	9 (0.66%)	166 (12.12%)	1,195 (87,23%)
Polar-negative	1,817 (100%)	0 (0.00%)	139 (7.65%)	1,678 (92.35%)
Lipidic-positive	4,190 (100%)	41 (0.98%)	269 (6.42%)	3,880 (92.60%)
Transcriptomics	**No. of features**	**Up**	**Down**	**Same**
AE, control plants at 45 DAT vs. control plants at 02 DAT				
Reference transcriptome	53,735 (100%)	1,347 (2.51%)	1,397 (2.60%)	50,991 (94.89%)
STS, stressed plants at 02 DAT vs. control plants at 02 DAT				
Reference transcriptome	53,735 (100%)	824 (1.53%)	487 (0.91%)	52,424 (97.56%)
LTS, stressed plants at 45 DAT vs. stressed plants at 02 DAT				
Reference transcriptome	53,735 (100%)	1,920 (3.57%)	2,229 (4.15%)	49,586 (92.28%)

Note. The differentially expressed peaks are those with a variable importance in projection (VIP) value ≥ 0.99 obtained from the partial least squares discriminant analysis model; adjusted *P* value (false discovery rate [FDR]) ≤ 0.05 of the Welch *t* test; Log_2 (fold change) $\neq 1$. Differentially expressed transcripts are those with an FDR ≤ 0.05, and Log_2 (fold change) ≥ 1 (upregulated) or Log_2 (fold change) ≤ -1 (downregulated).

Only two DEPs out of the 257 DEPs upregulated in STS did again on the LTS scenario (Table 2). On the other hand, 114 remained at the same level of expression as before, and 141 were downregulated. In the case of the 250 DEPs downregulated in STS, five upregulated, 238 maintained the same expression level as before, and seven downregulated further in the LTS scenario. At last, out of the 6,880 peaks not differently expressed in STS, 43 upregulated, and 426 downregulated in LTS, while 6,401 remained at the same level of expression as before.

All 976 peaks differentially expressed in STS, LTS, or both (Table 2) were then submitted to functional interpretation via analysis in the mass spectrometry Peaks to Pathway module as described in the Materials and Methods section. The combined mummichog (https://shuzhao-li.github.io/mummichog.org/) and Gene Set Enrichment Analysis pathway meta-analysis resulted in a list of 61 ranked pathways enriched in this group of DEPs. The pathways significantly perturbed in both algorithms were galactose metabolism, starch and sucrose metabolism, biosynthesis of unsaturated fatty acids, glycolysis, and gluconeogenesis, aminoacyl-tRNA biosynthesis, glycerophospholipid metabolism, lysine degradation, and glycosaminoglycan degradation pathways, with combined *p* values <.05 (Supplemental Figure S2G).

After applying the initial criteria of metabolite selection, as described in the Materials and Methods section, 107 DEPs with a hit to just one known compound were selected (Supplemental Table S2) and submitted to the pathway topology analysis module resulting in a list of 64 ranked pathways. The galactose metabolism (12 compounds), phenylpropanoid biosynthesis (14 compounds), ascorbate and aldarate metabolism (seven compounds), C5-branched dibasic acid metabolism (four compounds), and flavone and flavonol biosynthesis (five compounds) pathways came out at the top of this rank with an FDR < 0.05 (Supplemental Figure S2H).

3.3 | Gliricidia transcriptome under salinity stress

Based on the results of the morphophysiological characterization, as well as the ones from the metabolomics characterization, we then selected the following treatments for

TABLE 2 Differentially expressed peaks and features in the leaves of gliricidia plants submitted to salinity stress in two distinct scenarios: short-term stress (STS, control and the stress plants at 2 DAT) and long-term stress (LTS, stressed plants at 2 and 45 DAT)

Omics platform	STS, stressed plants at 2 DAT vs. control plants at 2 DAT		LTS, stressed plants at 45 DAT vs. stressed plants at 2 DAT	
Metabolomics polar-positive	1,380 peaks (100%)	93 peaks up (6.74%)	93 peaks (100%)	0 peak up (0.00%)
				40 peaks same (43.01%)
				53 peaks down (56.99%)
		1241 peaks same (89.93%)	1,231 peaks (100%)	8 peaks up (0.65%)
				1,111 peaks same (90.25%)
				112 peaks down (9.10%)
		46 peaks down (3.33%)	46 peaks (100%)	1 peak up (2.17%)
				44 peaks same (95.65%)
				1 peak down (2.17%)
Metabolomics polar-negative	1,817 peaks (100%)	37 peaks up (2.04%)	37 peaks (100%)	0 peak up (0.00%)
				17 peaks same (45.95%)
				20 peaks down (54.05%)
		1,751 peaks same (96.37%)	1,751 peaks (100%)	0 peak up (0.00%)
				1,633 peaks same (93.26%)
				118 peaks down (6.74%)
		29 peaks down (1.60%)	29 peaks (100%)	0 peak up (0.00%)
				28 peaks same (96.55%)
				1 peak down (3.45%)
Metabolomics lipidic-positive	4,190 peaks (100%)	127 peaks up (3.03%)	127 peaks (100%)	2 peak up (1.57%)
				57 peaks same (44.88%)
				68 peaks down (53.54%)
		3,888 peaks same (92.79%)	3,888 peaks (100%)	35 peaks up (0.90%)
				3,657 peaks same (94.06%)
				196 peaks down (5.04%)
		175 Peaks Down (4.18%)	175 peaks (100%)	4 peak up (2.29%)
				166 peaks same (94.86%)
				5 peaks down (2.86%)
Transcriptomics	53,735 features (100%)	824 features up (2.51%)	824 features (100%)	2 features up (0.24%)
				158 features same (19.17%)
				664 features down (80.58%)
		52,424 features same (94.89%)	52,424 features (100%)	1,654 features up (3.16%)
				49,215 features same (93.88%)
				1,555 features down (2.97%)
		487 features down (2.60%)	487 features (100%)	264 features up (54.21%)
				213 features same (43.74%)
				10 features down (2.05%)

Note. The differentially expressed peaks are those with a variable importance in projection (VIP) value ≥ 0.99, obtained from the partial least squares discriminant analysis model; adjusted *P* value (false discovery rate [FDR]) ≤ 0.05 of the Welch *t* test; and Log_2 (fold change) ≠ 1. Differentially expressed transcripts are those with an FDR ≤ 0.05, and Log_2 (fold change) ≥1 (upregulated) or Log_2 (fold change) ≤ −1 (downregulated).

transcriptomics analysis: samples treated with 0.0 and 0.8 g of NaCl per 100 g of the substrate at 2 and 45 DAT with three replicates per treatment.

The raw sequence data (24 fastq files) used in this study are in the Sequence Read Archive (SRA) database of the National Center for Biotechnology Information under 'Gliricidia sepium (Jacq.) Walp. Transcriptome,' BioProject number of PRJNA634354 (SUB7482509), BioSample SAMN14992839 (SUB7482677), and GS_BR01 (TaxID: 167663). The 24 fastq files generated using the 12

samples collected had 319,889,065 reads pairs or ~48 Gbases; 150 nucleotides per read (Supplemental Table S2). A total of 305,588,306 high-quality pairs of reads—with an average quality of reads ≥30 and the minimum length of 75 nucleotides—remained after preprocessing the raw sequence data (95.53%).

The assembled reference transcriptome (RT) has 53,735 features—the longest open reading frames per gene—ranging from 297 to 16,323 nucleotides in length. The high-quality sequences were then also used to perform the mapping, counting, and differential expression analysis against the RT. Prior to the submission to the functional annotation in OmicsBox, a BlastX analysis against the genome of soybean [*Glycine max* (L.) Merr.] [available at NCBI (Glycine_max_v2.1, BioProject PRJNA19861, BioSample SAMN00002965)] was performed in May 2020 (data not shown).

The pairwise differential expression analysis was then applied to measure the degree of a possible age effect using the AE data set, the differences in the short-term stress using the STS data set, and the differences in the long-term stress using the LTS data set. Differentially expressed genes are those with an FDR ≤ 0.05, and fold change > 1 (upregulated) or < 1 (downregulated). Out of the 53,735 features in the RT, 1,347 (2.51%) upregulated and 1,397 (2.60%) downregulated in the AE scenario. In the STS scenario, 824 (1.53%) upregulated and 487 (0.91%) downregulated. In the LTS scenario, 1,920 (3.57%) upregulated and 2,229 (4.15%) downregulated (Table 1).

Once it was clear that the number of DEGs was also <10%—as seen before for the DEPs (Table 1)—the same question emerged for DEGs: What is the fate in LTS of the DEGs from STS? Out of the 824 DEGs upregulated in STS, only two upregulated again in LTS, while 158 remained at the same level of expression as before and 664 downregulated (Table 2). In the case of the DEGs downregulated in STS, 264 upregulated, 213 maintained the same expression level as before, and 10 downregulated further in LTS.

A set of 12 DEGs, being two that upregulated twice—first in the STS and then again in the LTS as well—and 10 that downregulated twice, was chosen for further characterization (Figure 3). All 10 DEGs that downregulated twice, both in STS and LTS, showed a level of expression lower than in the AE scenario. It shows that salt stress also contributes to reducing the expression level (Figure 3a). The two DEGs that upregulated in the STS and then again in the LTS, also upregulated in the AE scenario; however, in the STS and LTS cumulative scenario, one DEG experienced a >260-fold increase, while in the AE scenario it had a ~51-fold increase; the same was true with the second DEG that experienced a 40-fold increase in the STS and LTS cumulative scenario and a ~21-fold increase in the AE one (Figure 3b).

Three out of the 12 DEGs got positive hits in BlastX to uncharacterized proteins in soybean. The remaining DEGs are homologs to genes coding for a WAT1-related protein At4g28040, a bidirectional sugar transporter SWEET14-like protein, a G-type lectin S-receptor-like serine/threonine-protein kinase At4g27290, a protein NIM1-INTERACTING 1-like, a protein SAR DEFICIENT 1 isoform X1, an F-box protein At2g27310, a Probable WRKY transcription factor 50, a VQ motif-containing protein 22, and a lysosomal Pro-X carboxypeptidase-like isoform X1 (Table 3).

3.4 | Integrating gliricidia metabolome and transcriptome data

Before performing an integrative analysis, we performed a correlation analysis employing a pairwise comparison of the three scenarios tested (AE, STS, and LTS), using the Log_2(FC) values obtained from the single-omics analysis. The 107 DEPs and a group of 5,672 DEGs—those up- and downregulated from all three scenarios—were then used in the correlation analysis.

The distribution of DEPs and DEGs in all three scenarios obeyed a normal distribution (Figure 4). Regarding DEPs, the correlation analysis revealed weak positive correlations between AE and STS (Figure 4a) and AE and LTS (Figure 4b) and a weak negative correlation between STS and LTS (Figure 4c). This weak negative correlation implies that the behavior seen for most of the 107 DEPs at STS does not repeat at LTS.

Regarding the DEGs, the correlation analysis between the three different scenarios showed no correlation between AE and STS (Figure 4d), a strong positive correlation between AE and LTS (Figure 4e), and a strong negative correlation between STS and LTS (Figure 4f). When comparing STS and LTS, the Log_2(FC) value at LTS results from the differential expressed changes seen between 2 and 45 DAT. For instance, a DEP or a DEG showing a $Log_2(FC) = 2.0$ at 45 DAT means that it upregulated 4× on the top of the change already observed at 2 DAT. A 4× increase in the STS would mean a 16× increase in the LTS compared with the expression level in the plants at 0.0 g of NaCl at 2 DAT.

These two groups of 5,672 DEGs and 107 DEPs were then submitted to the Omics Fusion (Brink et al., 2016) platform for integrative analysis to integrate transcripts and metabolites differentially expressed in gliricidia under salt stress. The phenylpropanoid pathway also came first in the rank of affected ones when using the Omics Fusion (Brink et al., 2016) platform, with 15 metabolites and six transcripts (three genes) (Figure 5). Eleven out of the 15 differentially expressed metabolites from this pathway were downregulated in LTS compared with their amounts in the STS (Figure 5a). In the case of the six differentially expressed transcripts, two upregulated and four downregulated in LTS when compared with STS (Figure 5b).

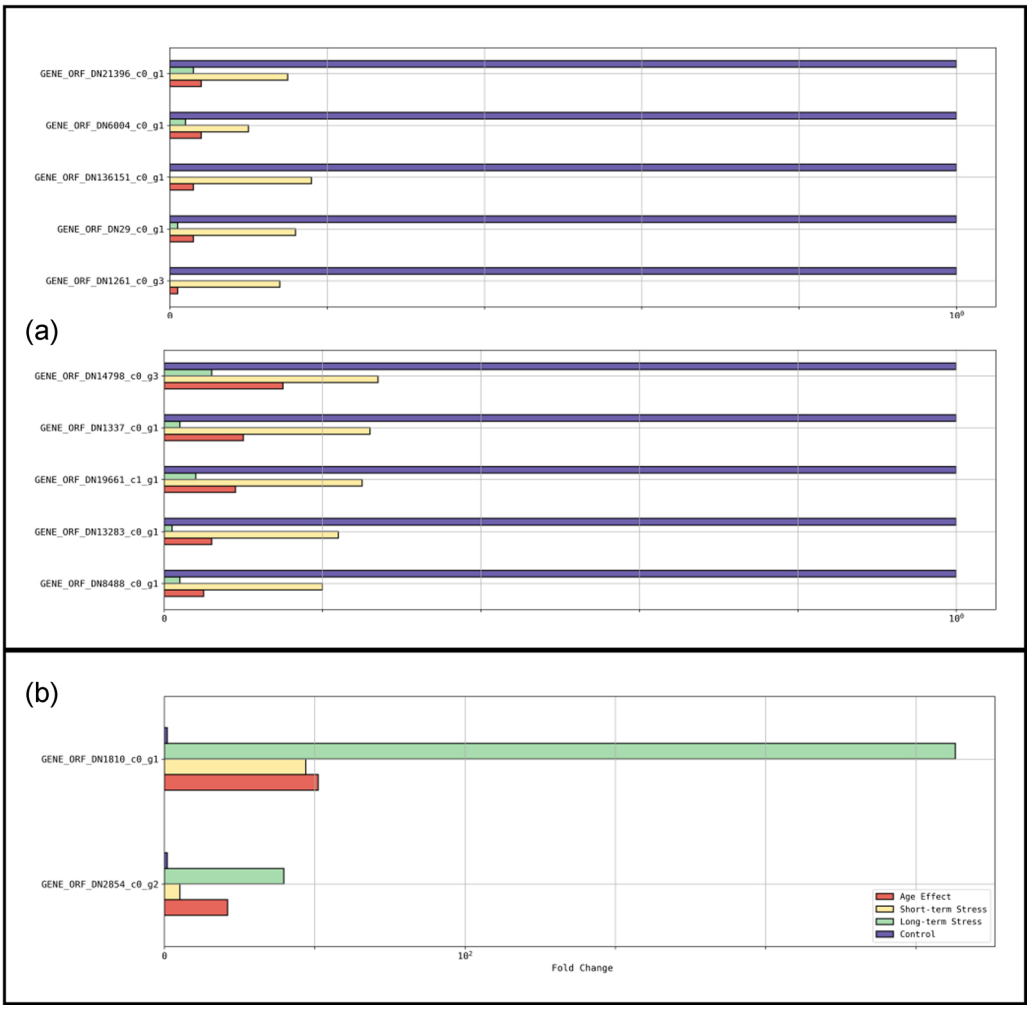

FIGURE 3 Expression profiles in percentage (*x* axis) of the 12 differentially expressed transcripts, being (a) two that upregulated twice in short-term stress (control and the stress plants at 2 d under salinity stress [DAT]) and long-term stress (stressed plants at 2 and 45 DAT) and (b) 10 that downregulated in the short-term and then again in the long-term stress resulted from submission of gliricidia plants to salinity stress compared with the control treatment (fold change = 1). Age effect is control plants at 2 and 45 DAT

The expression profiles of these 15 differentially expressed metabolites were then submitted to analysis in the AT data set. A one-way parametric ANOVA, with an adjusted *p* value (FDR) cutoff of 0.05, and the Fisher's least significant difference (Williams & Abdi, 2010) post hoc test was applied. All 15 metabolites had FDR $\leq$ 0.05 (data not shown).

Based on the expression profile in the AT data set, these metabolites could separate into different groups (Figure 6). The first group, upregulated at 2 DAT, had L-phenylalanine (C00079), L-tyrosine (C00082), and spermidine (C00315) in it; however, independent of the NaCl level, they had at 45 DAT an average peak intensity statistically similar to the plants submitted to 0.0 g of NaCl at 2 and 45 DAT. The expression profile of L-phenylalanine, an example of this group, is in Figure 6a.

Five metabolites from the phenylpropanoid biosynthesis pathway were downregulated in LTS, being two coniferyl alcohol derivates (C02666 and C05619), two paracoumaryl alcohol derivates (C02646 and C05608), and one sinapate derivate (C00482). Three of them (C02646, C02666, and C05608) showed strong upregulation under the highest level of salt (0.8 g of NaCl per 100 g of the substrate) at 2 DAT, getting, at 45 DAT, to an expression level similar to or lower than the one in the plants submitted to 0.0 g of NaCl at 2 and 45 DAT. The expression profile of coniferyl aldehyde, an example of the group, is in Figure 6b.

Another group of metabolites, comprised of C05838 (2-Coumarinate), C05839 (*beta*-D-glucosyl-2-coumarinate), and C10434 (5-O-caffeoylshikimic acid), showed a reduction in expression under salt stress (0.4 and 0.8 g of NaCl per 100 g of substrate) at 2 and 45 DAT; while C18069 (N1,N5,N10-tricoumaroyl spermidine) showed a reduction in expression under salt stress (0.4 and 0.8 g of NaCl per 100 g of substrate) only at 45 DAT. These four metabolites had expression levels under the highest NaCl dose at 45 DAT lower than in the plants submitted to 0.0 g of NaCl. The expression

TABLE 3 Gene ontology (GO) classification of the 12 differentially expressed transcripts, being two that upregulated twice: In short-term stress (STS, control and the stress plants at 2 d under salinity stress [DAT]) and long-term stress (LTS, stressed plants at two and 45 DAT) and 10 that downregulated in STS and then again in the LTS when gliricidia plants were submitted to salinity stress

Putative gene	Gene description	Biological process	Molecular function	Cellular component	InterPro IDs
GENE_ORF_DN1810_c0_g1	WAT1-related protein At4g28040	None	Transmembrane transporter activity (GO:0022857)	Membrane (GO:0016020); Integral component of membrane (GO:0016021)	IPR000620 (PFAM); IPR030184 (PANTHER); PTHR31218:SF244 (PANTHER); SSF103481 (SUPERFAMILY)
GENE_ORF_DN2854_c0_g2	Uncharacterized protein LOC113872764	None	Protein binding (GO:0005515)	None	IPR011990 (G3DSA:1.25.40.GENE3D); PTHR46816 (PANTHER); PTHR46816:SF1 (PANTHER); IPR001623 (CDD); IPR036869 (SUPERFAMILY); IPR011990 (SUPERFAMILY)
GENE_ORF_DN1261_c0_g3	Bidirectional sugar transporter SWEET14-like	None	None	Integral component of membrane (GO:0016021)	G3DSA:1.20.1280.290 (GENE3D); G3DSA:1.20.1280.290 (GENE3D); IPR004316 (PFAM); PTHR10791 (PANTHER); PTHR10791:SF22 (PANTHER)
GENE_ORF_DN13283_c0_g1	Uncharacterized protein LOC113853016	No GO Terms	No GO Terms	No GO Terms	IPR008889 (PFAM); mobidb-lite (MOBIDB_LITE); mobidb-lite (MOBIDB_LITE); mobidb-lite (MOBIDB_LITE); mobidb-lite (MOBIDB_LITE); PTHR33179:SF39 (PANTHER); IPR039609 (PANTHER)
GENE_ORF_DN1337_c0_g1	G-type lectin S-receptor-like serine/threonine-protein kinase At4g27290	Protein phosphorylation (GO:0006468); Recognition of pollen (GO:0048544)	Protein kinase activity (GO:0004672); Protein serine/threonine kinase activity (GO:0004674); ATP binding (GO:0005524)	None	G3DSA:1.10.510.10 (GENE3D); IPR021820 (PFAM); IPR000858 (PFAM); IPR036426 (G3DSA:2.90.10.GENE3D); IPR001480 (PFAM); IPR024171 (PIRSF); IPR001245 (PFAM); IPR003609 (PFAM); G3DSA:3.30.200.20 (GENE3D); PTHR32444 (PANTHER); PTHR32444:SF50 (PANTHER); IPR008271 (PROSITE_PATTERNS); IPR003609 (PROSITE_PROFILES); IPR001480 (PROSITE_PROFILES); IPR000719 (PROSITE_PROFILES); cd14066 (CDD); cd01098 (CDD); IPR001480 (CDD); IPR011009 (SUPERFAMILY); IPR036426 (SUPERFAMILY)

(Continues)

TABLE 3 (Continued)

Putative gene	Gene description	Biological process	Molecular function	Cellular component	InterPro IDs
GENE_ORF_DN136151_c0_g1	Protein NIM1-INTERACTING 1-like	Regulation of systemic acquired resistance (GO:0010112)	None	None	Coil (COILS); IPR031425 (PFAM); mobidb-lite (MOBIDB_LITE); mobidb-lite (MOBIDB_LITE); IPR031425 (PANTHER); PTHR33669:SF1 (PANTHER)
GENE_ORF_DN14798_c0_g3	Uncharacterized protein LOC111988154	None	Protein binding (GO:0005515)	None	IPR011990 (G3DSA:1.25.40.GENE3D); mobidb-lite (MOBIDB_LITE); mobidb-lite (MOBIDB_LITE); mobidb-lite (MOBIDB_LITE); PTHR26312 (PANTHER); PTHR26312:SF73 (PANTHER); IPR011990 (SUPERFAMILY)
GENE_ORF_DN19661_c1_g1	Protein SAR DEFICIENT 1 isoform X1	None	Calmodulin binding (GO:0005516)	None	IPR012416 (PFAM); PTHR31713:SF49 (PANTHER); IPR012416 (PANTHER)
GENE_ORF_DN21396_c0_g1	F-box protein At2g27310	None	Protein binding (GO:0005515)	None	IPR001810 (PFAM); G3DSA:1.20.1280.50 (GENE3D); PTHR33736 (PANTHER); IPR001810 (PROSITE_PROFILES); IPR036047 (SUPERFAMILY)
GENE_ORF_DN29_c0_g1	Probable WRKY transcription factor 50	Regulation of transcription, DNA-templated (GO:0006355)	DNA-binding transcription factor activity (GO:0003700); Sequence-specific DNA binding (GO:0043565)	None	IPR003657 (PFAM); IPR036576 (G3DSA:2.20.25.GENE3D); mobidb-lite (MOBIDB_LITE); mobidb-lite (MOBIDB_LITE); PTHR31221 (PANTHER); PTHR31221:SF144 (PANTHER); IPR003657 (PROSITE_PROFILES); IPR036576 (SUPERFAMILY)
GENE_ORF_DN6004_c0_g1	VQ motif-containing protein 22	No GO Terms	No GO Terms	No GO Terms	IPR008889 (PFAM); mobidb-lite (MOBIDB_LITE); mobidb-lite (MOBIDB_LITE); IPR039609 (PANTHER); PTHR33179:SF39 (PANTHER)
GENE_ORF_DN8488_c0_g1	Lysosomal Pro-X carboxypeptidase-like isoform X1	Proteolysis (GO:0006508)	Serine-type peptidase activity (GO:0008236)	None	IPR029058 (G3DSA:3.40.50.GENE3D); IPR042269 (G3DSA:1.20.120.GENE3D); IPR008758 (PFAM); PTHR11010:SF81 (PANTHER); PTHR11010 (PANTHER); IPR029058 (SUPERFAMILY); IPR029058 (SUPERFAMILY)

Note. The genes were classified into biological process, molecular function, and cellular component at the second level of GO classification.

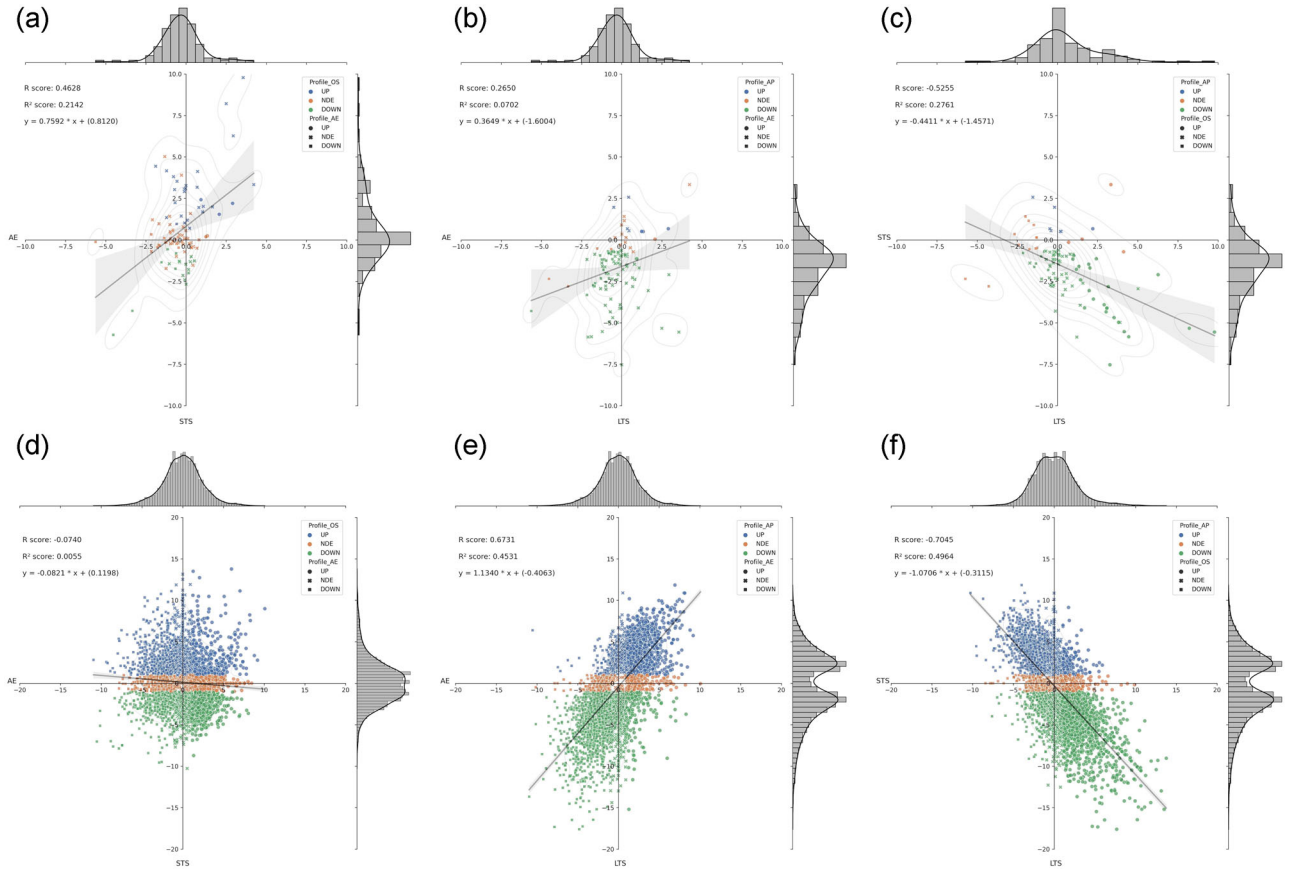

FIGURE 4 (a–c) Histogram and correlation analysis of the Log_2 (fold change) of 156 differentially expressed metabolites by pairwise comparison of three scenarios: age effect (AE, control plants at 2 and 45 d under salinity stress [DAT]); short-term stress (STS, control and the stress plants at 2 DAT); and long-term stress (LTS, stressed plants at 2 and 45 DAT). (d–f) Histogram and correlation analysis of the Log_2 (fold change) of 5,672 differentially expressed transcripts by pairwise comparison of three scenarios: AE (control plants at 2 and 45 DAT); STS (control and the stress plants at 2 DAT); and LTS (stressed plants at 2 and 45 DAT)

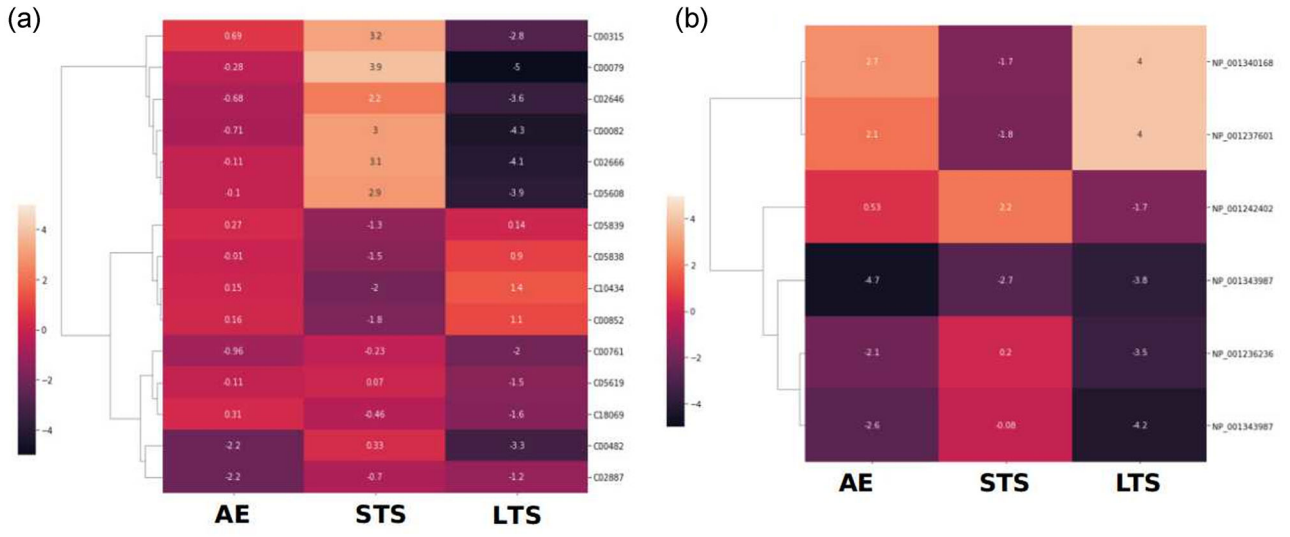

FIGURE 5 (a) Cluster heat map of 15 metabolites and (b) six transcripts from the phenylpropanoid pathway differentially expressed under salinity stress in the leaves of gliricidia plants. Hierarchical clustering of metabolites and transcripts with altered expression levels in three scenarios: age effect (AE, control plants at 2 and 45 d under salinity stress [DAT]); short-term stress (STS, control and the stress plants at 2 DAT); and long-term stress (LTS, stressed plants at 2 and 45 DAT). Metabolites identified by the KEGG id, and transcripts by Protein id. Log_2 (fold change) is presented in the center of each box

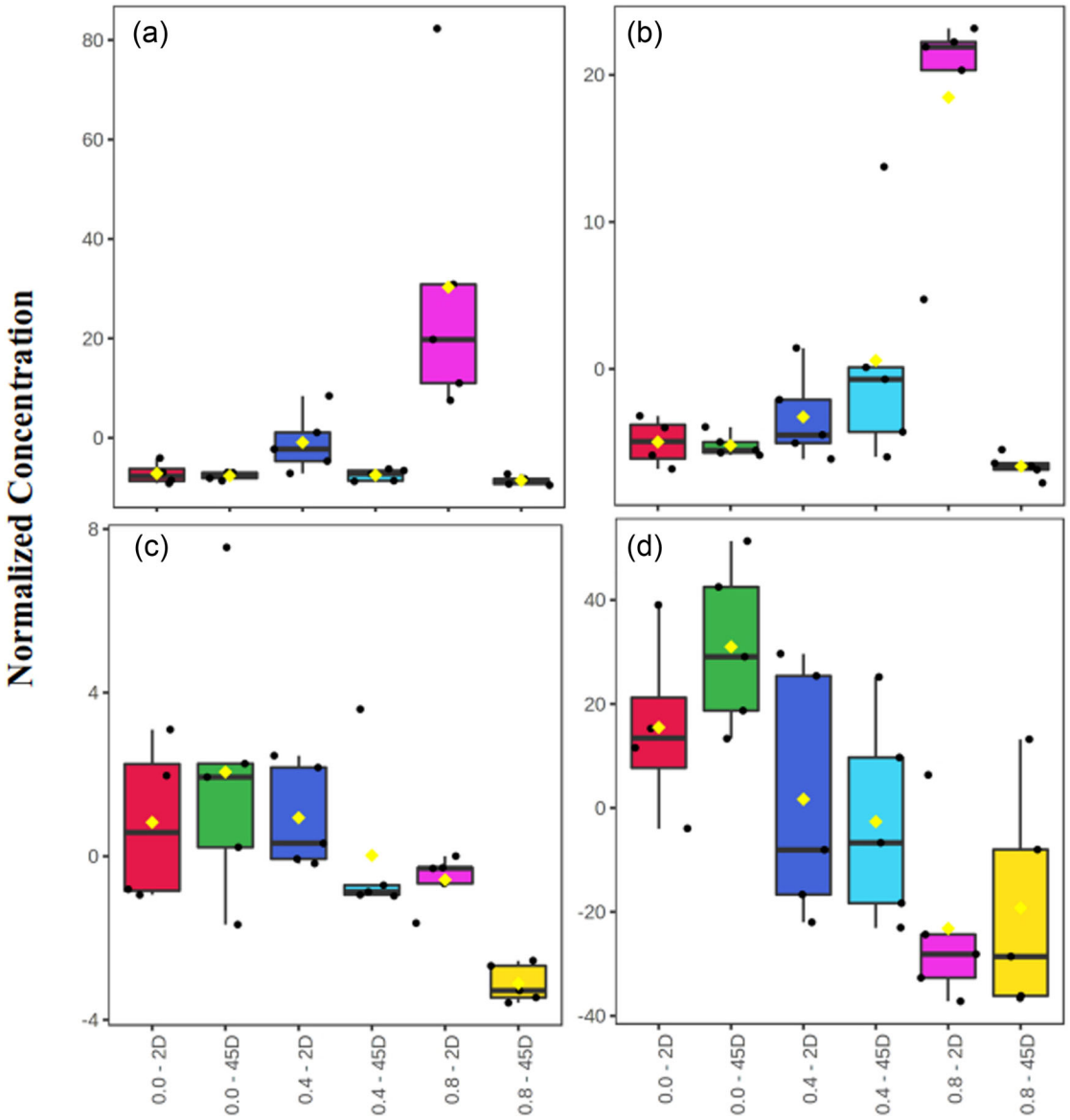

FIGURE 6 Box plot showing the original and normalized concentration of metabolites from the phenylpropanoid pathway differentially expressed under salinity stress in the leaves of gliricidia plants. The expression profiles of (a) L-phenylalanine, (b) coniferyl aldehyde, (c) N1,N5,N10-tricoumaroyl spermidine, (d) and *cis*-beta-D-glucosyl-2-hydroxycinnamate. The values represent the average of five replicates, and the bars represent the standard error of the mean. Treatments (*x* axis): 2 d under salinity stress [DAT]) or 45 DAT at 0.0, 0.4, or 0.8 g of NaCl per 100 g of substrate. The number on the top of the boxes indicates mass-to-charge ratio (*m*/*z*)

profiles of N1,N5,N10-tricoumaroyl spermidine, and *cis*-beta-D-glucosyl-2-hydroxycinnamate are shown in Figure 6c and 6d, respectively, as examples of the group.

4 | DISCUSSION

4.1 | Gliricidia response to a long-term, and extremely high salt concentration, stress

According to their response to salt stress, plants are glycophytes or halophytes. Halophytes can complete their life cycle in an environment where the salt concentration is equal or greater than 200 mM NaCl, approximately 20 dS m^{-1} at 25 ˚C, and glycophytes cannot do so (Flowers & Colmer, 2008; Flowers et al., 1986). So far, there is no report showing that gliricidia is indeed a halophyte species. Although, based on the results of this study, it is probably the case. Here gliricidia plants are grown under ~30 dS m^{-1} or more lost all their leaves in the first week after the stress onset; however, they started developing new leaves ~3 wk after the beginning of the stress and continued to produce more new leaves for additional 4 wk until the experiment ended. Considering that the salt stress level (≥30 dS m^{-1}) was the same throughout

the entire experiment; this is not a case of recovery from the stress. It is likely a case of adaptation to the stress condition (Acosta-Motos et al., 2017) that started with a very drastic measure taken by the plant (loss of all leaves) and followed by a transition to a state that allowed the plant to resume developing new leaves.

The NaCl added to the substrate, mainly the Na ion, is held on the surface of clay particles and organic matter (exchange points), resulting in an increase in exchangeable Na and in the cation exchange capacity (Supplemental Table S1). For that cation to be removed from the exchange points and to travel in the substrate profile, a force greater than the force that retains it would have to be applied. This is the principle behind remediating saline soils by applying large amount of gypsum and water. Therefore, pure water would not have sufficient strength to displace the salts from the exchange points and carry them through the substrate profile, reducing the salinity level in the substrate and, consequently, allowing the plant to resume growth.

Plants developed high phenotypic plasticity such as rapid responses to aggressive environmental factors and adaptations to changing environments (Ashapkin et al., 2020). Plants tolerant to NaCl respond to this stress by implementing changes that allow them to acclimate to salinity including morphological, physiological, and biochemical ones; an increase in the root/canopy ratio is one of these changes (Acosta-Motos et al., 2017). In the present study, it was possible to see an increase in the root/canopy ratio on gliricidia plants grown for 45 d under EC conditions of 15, 30, and 35 dS m^{-1} compared with 7.5 dS m^{-1}. The root/canopy ratio in the treatment with approximately ~40 dS m^{-1} was lower than at 35 dS m^{-1} (Figure 1).

Adapting to abiotic stresses is a critical step for the survival, and biomass accumulation, of sessile plants, particularly those perennials with a relatively long life cycle (Liu et al., 2019) such as gliricidia. Acosta-Motos et al. (2017) also point out that changes in the leaf anatomy are one of these changes that ultimately result in the prevention of leaf ion toxicity, thus maintaining the water status to limit water loss and protect the photosynthesis process. In this study, the evapotranspiration rate measured in gliricidia plants at 45 DAT in all saline levels was practically the same, and plants under stress from the two highest doses of salt use accumulated almost twice the amount of Na^+ in the leaves vs. the roots.

Understanding plant responses and adaptation mechanisms to severe salt stress conditions, such as the one from gliricidia reported in this study, is the key to improving crops economically important that could then serve biosaline agriculture. As a relatively new way of dealing with salinity in agriculture, biosaline agriculture uses cultivation systems for saline environments developed taking advantage of the ability of halophytes and salt-tolerant glycophyte plants to grow under saline conditions in combination with the use of saline soils, water resources, and better soil and water management (Duarte & Caçador, 2021; Ventura et al., 2015). To further boost biosaline agriculture initiatives wherever possible, it is vital to understand the physiological, metabolic, and biochemical responses of plants to salt stress and to mine the salt-tolerance-associated genetic resource in nature (Zhao et al., 2020).

Collecting, characterizing, and domesticating halophyte and salt-tolerant glycophyte species are the front runners to develop salt-tolerant crops. Besides that, there is the strategy to promote, whenever possible, the vertical or horizontal transference of this trait to crops economically important [e.g., soybean, wheat (*Triticum aestivum* L.), corn (*Zea mays* L.), rice (*Oryza sativa* L.), sugarcane (*Saccharum officinarum* L.), to name a few]. The novel CRISPR–Cas9 genome editing system will be a key factor in achieving a more precise horizontal transfer, reducing, to a certain extent, the need for some biosafety analysis demanded nowadays for genetically modified plants (Zhu et al., 2020).

The multiomics systems biology research (Jamil et al., 2020) will expand the existing knowledge on the response of plant species to the environment, including salt stress. It will do so empowered using transcriptomics, proteomics, and metabolomics data sets, facilitating in the long run either conventional or biotechnological breeding efforts toward developing salt-tolerant crops. Besides reporting for the first time the ability of gliricidia plants to adapt to a severe salt stress condition, the present study is also the first one to integrate metabolomics and transcriptomics data to gain a better understanding of this species short- and long-term responses to such an abiotic condition.

4.2 | A role for the phenylpropanoid biosynthesis pathway in the response to salinity stress

In the present study, the phenylpropanoid pathway came as the first ranked pathway in two distinct analyses. From the pathway analysis module in MetaboAnalyst 4.0 (Chong & Xia, 2020; Chong et al., 2019), 13 out of the 46 metabolites of this pathway were among the metabolites in the list of 107 differentially expressed compounds submitted to analysis. Then, using the Omics Fusion (Brink et al., 2016) platform for integrative analysis to integrate transcripts and metabolites differentially expressed in gliricidia under salt stress, this pathway came first with 15 metabolites and five transcripts (three genes).

These results put this pathway, and consequently the metabolites and genes in it, in the center of interest to further study the response of gliricidia to salinity stress. The gliricidia adaptation phenomena to salinity stress described in this study is an interesting case study for further understanding the flux

control in this complex biosynthetic pathway as well as to the identification of targets for biotechnological manipulation.

There are three principal kinds of secondary metabolites biosynthesized by plants: phenolic compounds, terpenoids and isoprenoids, and alkaloids and glucosinolates. The former represents the largest group of secondary metabolites in plants (Sharma et al., 2019; Santos-Sánchez et al., 2019). Phenylpropanoids are phenolics compounds derived from phenylalanine and tyrosine and are involved in plant defense, structural support, and survival (Deng & Lu, 2017; Sharma et al., 2019; Santos-Sánchez et al., 2019).

According to Sharma et al. (2019), abiotic stresses disturb the balance between reactive oxygen species (ROS) generation and scavenge and accelerate ROS propagation that damages nucleic acids, proteins, carbohydrates, and lipids, eventually leading to cell death. Plants growing under stressful environments can biosynthesize more phenolic compounds than plants growing under normal conditions; these compounds have antioxidative properties and can scavenge free radicals, resulting in a reduction of cell membrane peroxidation, hence protecting plant cells from ill effects of oxidative stress (Sharma et al., 2019).

Phenylpropanoid metabolism is at the interface of primary and secondary metabolism. The phenylpropanoid pathway, also known as the phenylalanine–hydroxycinnamate pathway, is likely the most studied secondary metabolism pathway in plants. Plants exhibiting increased polyphenols synthesis under abiotic stresses usually show better adaptability to limiting environments (Kumar et al., 2019; Sharma et al., 2019). Based on chemical structures, there are five phenylpropanoid groups: flavonoids, monolignols, phenolic acids, stilbenes, and coumarins (Deng & Lu, 2017). Flavonoids, monolignols, coumarins, and stilbenes can act as defensive components in plants against various biotic and abiotic stresses, and salicylic acid is a phenolic phytohormone that acts as a signaling molecule in plant response to diverse biotic and abiotic stresses (Deng & Lu, 2017).

All 15 metabolites from the phenylpropanoid biosynthesis pathway differentially expressed in the leaves of gliricidia plants under very high salt stress (~35 dS m^{-1}) at 45 DAT show an average peak intensity similar to or lower than the one in the plants under very low salt stress (7.5 dS m^{-1}). These results show that it is likely that these 15 metabolites have no role in maintaining the status of salt stress-adapted plants described above for gliricidia. However, as several of them were differentially expressed—either up or downregulated—in the STS phase (2 DAT), it signals a possible role of the metabolites from the phenylpropanoid biosynthesis pathway in this initial stage of salt stress.

It is necessary to state that this present study has focused on the metabolome and transcriptome of the leaves of gliricidia plants under salt stress. It did by trying to understand what was different in the new leaves produced after the plants adapted to a very high salt stress level. A similar or broader multiomics study of the roots certainly will add additional insights into the process of understanding the adaptation phenomena seen in these gliricidia plants.

Phenylalanine ammonia-lyase, cinnamate-4-hydroxylase, and 4-coumarate-CoA ligase are the enzymes that catalyze the first three steps in the reaction sequence of the phenylpropanoid pathway; genetic inhibition of their respective genes significantly reduces the phenolic compounds content in several plant species (Feduraev et al., 2020). The Omics Fusion (Brink et al., 2016) platform showed, via a transcriptome and metabolome integrative analysis, that five transcripts (three genes) coding for proteins present in the phenylpropanoid pathway were differentially expressed in gliricidia leaves under salt stress either in the STS or LTS (Figure 5b).

The transcriptomic analysis revealed that two of these genes (*Phenylalanine ammonia-lyase* [*PAL*] and *4-coumarate-CoA ligase* [*4CL*]) were differentially expressed in plants under salt stress at 45 DAT. The homolog of the *PAL* gene in gliricidia had its normalized counts per million reduced approximately sixfold because of AE (data not shown); however, it underwent an additional threefold reduction because of the salt stress. No significant reduction was seen for the *PAL* gene in gliricidia at 2 DAT. The *4CL* gene showed a fourfold fall in counts per million because of AE and an additional twofold reduction because of the salt stress (data not shown). These results show that the low amount of L-phenylalanine in the leaves of salt-stress-adapted gliricidia plants is not due to an overexpression of the *PAL* gene and the consequent trans-cinnamate (C00423) production.

The remaining three transcripts coded for homologs of peroxidase genes in soybean, the *PER1*, the *PRX2*, and the *LOC100817540* genes. The *PER1* and *PRX2* genes encode proteins with peroxidase activity that respond to oxidative stress. In plants, the cellular regulation through a complex network involving redox input elements, transmitters, targets, and sensory proteins, such as peroxiredoxins (Prx), is part of the antioxidant defenses (Tovar-Méndez et al., 2011; Perkins et al., 2015; Rhee, 2016).

Peroxiredoxin constitutes a large and highly conserved family of peroxidases that catalyze the reduction of H_2O_2, alkyl hydroperoxides, and peroxynitrite to water, alcohols, and nitrite, respectively, and contain one or two Cys residues at the active site and usually function as monomers or dimers (Perkins et al., 2015; Rhee, 2016). There are four types of Prx enzymes in plants (1CPrx, 2CPrx, PrxII, and PrxQ) that protect the nuclei, plastids, cytosol, and the mitochondria against excess ROS in stressful conditions and are also implicated in redox signaling (Tovar-Méndez et al., 2011).

In the present study, the homolog of the *PER1* gene in gliricidia had its expression level increased by 6.34-fold because of the AE, decreased by 3.25-fold at short-term, and increased by 15.72-fold at LTS. At 45 DAT, its expression level in the

stressed plants was ~75% of that in the plants under the lowest salt stress level use at the same age. On the other hand, the homolog of the *PRX2* gene in gliricidia had its expression level increased by 4.16-fold because of AE, decreased by 3.58-fold at STS, and increased by 16.14-fold at LTS. At 45 DAT, its expression level in the stressed plants was ~10% higher than the one under the lowest salt stress level use at the same age. The homolog of the *LOC100817540* gene in gliricidia increased 1.44-fold because of the AE and 4.52-fold because of STS. At 45 DAT, its expression level in the stressed plants was about the same as in the plants under the lowest salt stress level use at the same age.

These results show that whether any of these three peroxidases would play a role in the response of gliricidia plants to the salt stress, it probably would be the protein coded by the homolog of the *LOC100817540* gene and it would be in the short-term. In the long-term, on the other hand, it seems that none of them has any role in maintaining the status of salt-stress-adapted plants described above for gliricidia.

4.3 | Genes up- or downregulated in STS and LTS

The two genes upregulated at the STS and LTS scenarios (Table 2) code for an uncharacterized and a bidirectional sugar transporter SWEET14-like protein, respectively. Sugars transporters perform a role in development, metabolism, growth, and homeostasis in plants, and there are three distinct superfamilies of sugars transporters: the glucose transporters (GLUTs), the sodium solute symporter family such as sodium–glucose cotransporters (SGLTs), and Sugar Will Eventually be Exported Transporter (SWEET) proteins (Jeena et al., 2019). The proteins from the SWEET family contain seven predicted transmembrane domains with two internal triple-helix bundles. The plant genome contains about 20 SWEET paralogs, which are differentially expressed in tissues and are involved in the transport of different sugar molecules (Jeena et al., 2019).

Salinity stress (150 mM of NaCl) upregulated *SWEET14* gene in the stem of *Arabidopsis* plants and downregulated in the leaves of rice (Chen et al., 2019; Sellami et al., 2019). The gene coding for the bidirectional sugar transporter SWEET14-like protein in gliricidia had its expression level increased by 51.21-fold because of the AE, 47.06-fold because of STS, and 5.59-fold because of LTS (on the top of what had already increased in the STS), resulting in an increase of 211.86 times in the level of expression due exclusively to the salt stress already discounting the AE or 513.70% higher than in the control plant at 45 DAT. These results show that this protein might play a role in gliricidia response at STS and LTS. The same is true for the gene coding for an uncharacterized protein, which expression level increased almost 20 times only as a result of the salt stress and already discounting the AE.

Among the 10 genes downregulated twice, at the STS and LTS scenarios (Table 2), two code for uncharacterized proteins. The remaining eight genes code for a Probable WRKY transcription factor 50, a WAT1-related protein, a G-type lectin S-receptor-like serine/threonine-protein kinase, a NIM1-INTERACTING 1-like protein, a SAR Deficient 1 protein, an F-box protein, a VQ motif-containing protein, and a lysosomal Pro-X carboxypeptidase-like isoform X1. For all of them, most of the decrease in the level of expression at 45 DAT resulted from the AE, with a minor contribution of the salt stress (data not shown).

5 | CONCLUSION

Depending on the amount of NaCl used in a substrate salinization protocol employed, gliricidia plants showed two different responses:

1. Plants grown under salinity stress up to 15 dS m^{-1} for 45 d did not show any visual symptoms of stress on the aerial parts, such as leaf wilt, yellowing, burning, or falling, although they experienced a reduction in the canopy and roots biomass yield. This response was named tolerance response.
2. Plants grown on a substrate with ≥30 dS m^{-1} lost all their leaves in the first week after the stress onset; however, ~2 wk after that, they started to develop new leaves from the lateral meristems that continued throughout the rest of the experiment. This response was named adaptation response.

The analysis of the transcriptome and metabolome data sets under three distinct scenarios—AE, STS, and LTS—and the integration of these two omics profiles pointed to a central role of the phenylpropanoid biosynthesis pathway in the short-term response of gliricidia to salinity stress but not in the long-term.

The transcriptomics analysis led to the identification of 5,672 differentially expressed transcripts (up- and downregulated) but only 12 differentially expressed in both the STS and LTS scenarios. Two of them do code for proteins that might play a role in gliricidia response at both STS and LTS.

ACKNOWLEDGMENTS

Thalliton Luiz Carvalho da Silva and Vivianny Nayse Belo Silva contributed equally to this study. The authors acknowledge funding to T.L.C.S., V.N.B.S., I.O.B., and J.C.R.N. by the Coordination for the Improvement of Higher Education Personnel (CAPES), via the Graduate Program in Plant Biotechnology at the Federal University of Lavras (UFLA)

and the Graduate Program in Chemistry at the Federal University of Goiás (UFG). The authors disclose receipt of the following financial support for the research, authorship, and/or publication of this article: the grant (01.13.0315.00 - DendePalm Project) for this study was awarded by the Brazilian Ministry of Science, Technology, and Innovation (MCTI) via the Brazilian Research and Innovation Agency (FINEP). The authors confirm that the funder had no influence over the study design, the content of article, or selection of this journal.

AUTHOR CONTRIBUTIONS

Thalliton Luiz Carvalho da Silva: Data curation; Formal analysis; Investigation; Methodology; Writing-original draft. Vivianny Nayse Belo Silva: Data curation; Formal analysis; Investigation; Methodology; Writing-original draft. Ítalo de Oliveira Braga: Data curation; Formal analysis. Jorge Candido Rodrigues Neto: Data curation; Formal analysis. André Pereira Leão: Investigation; Methodology. José Antônio de Aquino Ribeiro: Investigation; Methodology. Leonardo Fonseca Valadares: Conceptualization; Methodology. Patrícia Verardi Abdelnur: Conceptualization; Methodology. Carlos Antônio Ferreira de Sousa: Conceptualization; Methodology; Writing-original draft. Manoel Teixeira Souza Júnior: Conceptualization, Funding acquisition, Project administration, Supervision, Writing-original draft, Writing-review & editing.

CONFLICTS OF INTEREST

The authors declare no conflicts of interest.

ORCID

Manoel Teixeira Souza Jr. https://orcid.org/0000-0002-6590-9333

REFERENCES

Acosta-Motos, J., Ortuño, M., Bernal-Vicente, A., Diaz-Vivancos, P., Sanchez-Blanco, M., & Hernandez, J. (2017). Plant responses to salt stress: Adaptive mechanisms. *Agronomy*, *7*, 18. https://doi.org/10.3390/agronomy7010018

Anders, S., Pyl, P. T., & Huber, W. (2015). HTSeq–A Python framework to work with high-throughput sequencing data. *Bioinformatics*, *31*, 166–169. https://doi.org/10.1093/bioinformatics/btu638

Andrews, S. (2010). *FastQC: A quality control tool for high throughput sequence data*. http://www.bioinformatics.babraham.ac.uk/projects/fastqc/

Ashapkin, V. V., Kutueva, L. I., Aleksandrushkina, N. I., & Vanyushin, B. F. (2020). Epigenetic Mechanisms of Plant Adaptation to Biotic and Abiotic Stresses. *International Journal of Molecular Sciences*, *21*, 7457. https://doi.org/10.3390/ijms21207457

Ashraf, M., Shahzad, S. M., Imtiaz, M., & Rizwan, M. S. (2018). Salinity effects on nitrogen metabolism in plants – focusing on the activities of nitrogen metabolizing enzymes: A review. *Journal of Plant Nutrition*, *41*, 1065–1081, https://doi.org/10.1080/01904167.2018.1431670

Askenazi, M., Driggers, E. M., Holtzman, D. A., Norman, T. C., Iverson, S., Zimmer, D. P., Boers, M. -. E., Blomquist, P. R., Martinez, E. J., Monreal, A. W., Feibelman, T. P., Mayorga, M. E., Maxon, M. E., Sykes, K., Tobin, J. V., Cordero, E., Salama, S. R., Trueheart, J., Royer, J. C., & Madden, K. T. (2003). Integrating transcriptional and metabolite profiles to direct the engineering of lovastatin-producing fungal strains. *Nature biotechnology*, *21*, 150–156. https://doi.org/10.1038/nbt781

BioBam. (2019). *OmicsBox–Bioinformatics made easy*. https://www.biobam.com/omicsbox

Bolger, A. M., Lohse, M., & Usadel, B. (2014). Trimmomatic: A flexible trimmer for Illumina sequence data. *Bioinformatics*, *30*, 2114–2120. https://doi.org/10.1093/bioinformatics/btu170

Bresler, E., McNeal, B. L., & Carter, D. L. (1982). *Saline and sodics soils: Principles-dynamics-modeling*. Springer-Verlag. https://doi.org/10.1007/978-3-642-68324-4

Brink, B. G., Seidel, A., Kleinbölting, N., Nattkemper, T. W., & Albaum, S. P. (2016). Omics fusion—A platform for integrative analysis of omics data. *Journal of Integrative Bioinformatics*, *13*, 296. https://doi.org/10.2390/biecoll-jib-2016-296

Cavill, R., Jennen, D., Kleinjans, J., & Briedé, J. J. (2016). Transcriptomic and metabolomic data integration. *Briefings in Bioinformatics*, *17*, 891–901. https://doi.org/10.1093/bib/bbv090

Chen, G., Hu, J., Dong, L., Zeng, D., Guo, L., Zhang, G., Zhu, L., & Qian, Q. (2019). The tolerance of salinity in rice requires the presence of a functional copy of *FLN2*. *Biomolecules*, *10*, 17. https://doi.org/10.3390/biom10010017

Chong, J., Wishart, D. S., & Xia, J. (2019). Using MetaboAnalyst 4.0 for comprehensive and integrative metabolomics data analysis. *Current Protocols in Bioinformatics*, *68*, e86. https://doi.org/10.1002/cpbi.86

Chong, J., & Xia, J. (2020). Using MetaboAnalyst 4.0 for Metabolomics Data Analysis, Interpretation, and Integration with Other Omics Data. *Methods in Molecular Biology*, *2104*, 337–360. https://doi.org/10.1007/978-1-0716-0239-3_17

Deng, Y., & Lu, S. (2017). Biosynthesis and Regulation of Phenylpropanoids in Plants. *Critical Reviews in Plant Sciences*, *36*, 257–290, https://doi.org/10.1080/07352689.2017.1402852

Diouf, A., Ndiaye, M., Fall-Ndiaye, M. A., & Diop, T. A. (2017). Maize crop N uptake from organic material of *Gliricidia sepium* coinoculated with *Rhizobium* and arbuscular mycorrhizal fungus in sub-Saharian Africa sandy soil. *American Journal of Plant Sciences*, *8*, 428–440. https://doi.org/10.4236/ajps.2017.83029

Dobin, A., Davis, C. A., Schlesinger, F., Drenkow, J., Zaleski, C., Jha, S., Batut, P., Chaisson, M., & Gingeras, T. R. (2013). STAR: Ultrafast universal RNA-seq aligner. *Bioinformatics*, *29*, 15–21. https://doi.org/10.1093/bioinformatics/bts635

Duarte, B., & Caçador, I. (2021). Iberian halophytes as agroecological solutions for degraded lands and biosaline agriculture. *Sustainability*, *13*, 1005, https://doi.org/10.3390/su13021005

FAO – Food and Agriculture Organization. (2011). *FAO in the 21st century - ensuring food security in a changing world*. www.fao.org/3/i2307e/i2307e.pdf

Feduraev, P., Skrypnik, L., Riabova, A., Pungin, A., Tokupova, E., Maslennikov, P., & Chupakhina, G. (2020). Phenylalanine and tyrosine as exogenous precursors of wheat (*Triticum aestivum* L.) secondary metabolism through PAL-associated pathways. *Plants*, *9*, 476. https://doi.org/10.3390/plants9040476

Flowers, T. J., & Colmer, T. D. (2008). Salinity tolerance in halophytes. *The New phytologist*, *179*, 945–963. https://doi.org/10.1111/j.1469-8137.2008.02531.x

Flowers, T. J., Hajibagheri, M. A., & Clipson, N. J. W. (1986). Halophytes. *The Quarterly Review of Biology*, *61*, 313–337. https://doi.org/10.1086/415032

Gotz, S., Garcia-Gomez, J. M., Terol, J., Williams, T. D., Nagaraj, S. H., Nueda, M. J., Robles, M., Talon, M., Dopazo, J., & Conesa, A. (2008). High-throughput functional annotation and data mining with the Blast2GO suite. *Nucleic acids research*, *36*, 3420–3435. https://doi.org/10.1093/nar/gkn176

Gowda, H., Ivanisevic, J., Johnson, C. H., Kurczy, M. E., Benton, H. P., Rinehart, D., Nguyen, T., Ray, J., Kuehl, J., Arevalo, B., Westenskow, P. D., Wang, J., Arkin, A. P., Deutschbauer, A. M., Patti, G. J., & Siuzdak, G. (2014). Interactive XCMS online: Simplifying advanced metabolomic data processing and subsequent statistical analyses. *Analytical Chemistry*, *86*, 6931–6939. https://doi.org/10.1021/ac500734c

Grabherr, M. G., Haas, B. J., Yassour, M., Levin, J. Z., Thompson, D. A., Amit, I., Adiconis, X., Fan, L., Raychowdhury, R., Zeng, Q., Chen, Z., Mauceli, E., Hacohen, N., Gnirke, A., Rhind, N., Di Palma, F., Birren, B. W., Nusbaum, C., Lindblad-Toh, K., … Regev, A. (2011). Full-length transcriptome assembly from RNA-Seq data without a reference genome. *Nature biotechnology*, *29*, 644–652. https://doi.org/10.1038/nbt.1883

Hoefgen, R., & Nikiforova, V. J. (2008). Metabolomics integrated with transcriptomics: Assessing systems response to sulfur-deficiency stress. *Physiologia Plantarum*, *132*, 190–198. https://doi.org/10.1111/j.1399-3054.2007.01012.x

Jamil, I. N., Remali, J., Azizan, K. A., Nor Muhammad, N. A., Arita, M., Goh, H. -. H., & Aizat, W. M. (2020). Systematic multi-omics integration (MOI) approach in plant systems biology. *Frontiers in Plant Science*, *11*, 944. https://doi.org/10.3389/fpls.2020.00944

Jeena, G. S., Kumar, S., & Shukla, R. K. (2019). Structure, evolution and diverse physiological roles of SWEET sugar transporters in plants. *Plant Molecular Biology*, *100*, 351–365. https://doi.org/10.1007/s11103-019-00872-4

Kumar, S., Kumar, R., Pal, A., & Chopra, D. S. (2019). Chapter 16 – Enzymes. In E. M. Yahia (Ed.) *Postharvest physiology and biochemistry of fruits and vegetables* (pp. Pages 335–358). Woodhead Publishing. https://doi.org/10.1016/B978-0-12-813278-4.00016-6

Langmead, B., & Salzberg, S. L. (2012). Fast gapped-read alignment with Bowtie 2. *Nature methods*, *9*, 357–359. https://doi.org/10.1038/nmeth.1923

Li, S., Park, Y., Duraisingham, S., Strobel, F. H., Khan, N., Soltow, Q. A., Jones, D. P., & Pulendran, B. (2013). Predicting network activity from high throughput metabolomics. *PLoS Computational Biology*, *9*, e1003123. https://doi.org/10.1371/journal.pcbi.1003123

Liu, J.-G., Han, X., Yang, T., Cui, W.-H., Wu, A.-M., Fu, C.-X., Wang, B.-C., & Liu, L.-J. (2019). Genome-wide transcriptional adaptation to salt stress in *Populus*. *BMC Plant Biology*, *19*, 367. https://doi.org/10.1186/s12870-019-1952-2 PMID: 31429697

Perkins, A., Nelson, K. J., Parsonage, D., Poole, L. B., & Karplus, P. A. (2015). Peroxiredoxins: Guardians against oxidative stress and modulators of peroxide signaling. *Trends in Biochemical Sciences*, *40*, 435–445. https://doi.org/10.1016/j.tibs.2015.05.001

Phang, J. M., Liu, W., & Zabirnyk, O. (2010). Proline metabolism and microenvironmental stress. *Annual Review of Nutrition*, *30*, 441–463. https://doi.org/10.1146/annurev.nutr.012809.104638

Rahman, M. A., Das, A. K., Saha, S. R., Uddin, M. M., & Rahman, M. M. (2019). Morpho-physiological response of *Gliricidia sepium* to seawater-induced salt stress. *The Agriculturists*, *17*, 66–75. https://doi.org/10.3329/agric.v17i1-2.44697

Rai, A., Rai, M., Kamochi, H., Mori, T., Nakabayashi, R., Nakamura, M., Suzuki, H., Saito, K., & Yamazaki, M. (2020). Multiomics-based characterization of specialized metabolites biosynthesis in *Cornus officinalis*. *DNA research : an international journal for rapid publication of reports on genes and genomes*, *27*, dsaa009. https://doi.org/10.1093/dnares/dsaa009

Rhee, S. G. (2016). Overview on peroxiredoxin. *Molecules and cCells*, *39*, 1–5. https://doi.org/10.14348/molcells.2016.2368

Robinson, M. D., McCarthy, D. J., & Smyth, G. K. (2010). edgeR: A Bioconductor package for differential expression analysis of digital gene expression data. *Bioinformatics*, *26*, 139–140. https://doi.org/10.1093/bioinformatics/btp616

Rodrigues-Neto, J. C., Correia, M. V., Souto, A. L., Ribeiro, J. A. D. A., Vieira, L. R., Souza, M. T., Rodrigues, C. M., & Abdelnur, P. V. (2018). Metabolic fingerprinting analysis of oil palm reveals a set of differentially expressed metabolites in fatal yellowing symptomatic and non-symptomatic plants. *Metabolomics*, *14*, 142. https://doi.org/10.1007/s11306-018-1436-7

Santos-Sánchez, N. F., Salas-Coronado, R., Hernandez-Carlos, B., & Villanueva-Cañongo, C. (2019). Shikimic acid pathway in biosynthesis of phenolic compounds. In M. Soto-Hernández, R. García-Mateos, & M. Palma-Tenango (Eds.), *Plant physiological aspects of phenolic compounds*. IntechOpen. https://doi.org/10.5772/intechopen.83815

Sellami, S., Le Hir, R., Thorpe, M. R., Vilaine, F., Wolff, N., Brini, F., & Dinant, S. (2019). Salinity effects on sugar homeostasis and vascular anatomy in the stem of the *Arabidopsis Thaliana* inflorescence. *International Journal of Molecular Sciences*, *20*, 3167. https://doi.org/10.3390/ijms20133167

Shahid, S. A., Zaman, M., & Heng, L. (2018). Soil salinity: Historical perspectives and a world overview of the problem. In *Guideline for salinity assessment, mitigation and adaptation using nuclear and related techniques*. Springer. https://doi.org/10.1007/978-3-319-96190-3_2

Sharma, A., Shahzad, B., Rehman, A., Bhardwaj, R., Landi, M., & Zheng, B. (2019). Response of phenylpropanoid pathway and the role of polyphenols in plants under abiotic stress. *Molecules*, *24*, 2452. https://doi.org/10.3390/molecules24132452

Subramanian, A., Tamayo, P., Mootha, V. K., Mukherjee, S., Ebert, B. L., Gillette, M. A., Paulovich, A., Pomeroy, S. L., Golub, T. R., Lander, E. S., & Mesirov, J. P. (2005). Gene set enrichment analysis: A knowledge-based approach for interpreting genome-wide expression profiles. *Proceedings of the National Academy of Sciences*, *102*, 15545–15550. https://doi.org/10.1073/pnas.0506580102

Tautenhahn, R., Patti, G. J., Rinehart, D., & Siuzdak, G. (2012). XCMS Online: A web-based platform to process untargeted metabolomic data. *Analytical Chemistry*, *84*, 5035–5039. https://doi.org/10.1021/ac300698c

Tovar-Méndez, A., Matamoros, M. A., Bustos-Sanmamed, P., Dietz, K. -. J., Cejudo, F. J., Rouhier, N., Sato, S., Tabata, S., & Becana, M. (2011). Peroxiredoxins and NADPH-dependent thioredoxin systems in the model legume *Lotus japonicus*. *Plant physiology*, *156*, 1535–1547. https://doi.org/10.1104/pp.111.177196

Urbanczyk-Wochniak, E., Luedemann, A., Kopka, J., Selbig, J., Roessner-Tunali, U., Willmitzer, L., & Fernie, A. R. (2003). Parallel analysis of transcript and metabolic profiles: A new approach in systems biology. *EMBO Reports*, *4*, 989–993. https://doi.org/10.1038/sj.embor.embor944

Van Zelm, E., Zhang, Y., & Testerink, C. (2020). salt tolerance mechanisms of plants. *Annual Review of Plant Biology*, *71*, 403–433. https://doi.org/10.1146/annurev-arplant-050718-100005

Vargas, L. H. G., Neto, J. C. R., De Aquino Ribeiro, J. A., Ricci-Silva, M. E., Souza, M. T., Rodrigues, C. M., De Oliveira, A. E., & Abdelnur, P. V. (2016). Metabolomics analysis of oil palm (*Elaeis guineensis*) leaf: Evaluation of sample preparation steps using UHPLC–MS/MS. *Metabolomics*, *12*, 153. https://doi.org/10.1007/s11306-016-1100-z

Vargas, R., Pankova, E. I., Balyuk, S. A., Krasilnikov, P. V., & Khasankhanova, G. M. (Eds.). (2018). *Handbook for saline soil management*. FAO. www.fao.org/3/i7318en/I7318EN.pdf

Ventura, Y., Eshel, A., Pasternak, D., & Sagi, M. (2015). The development of halophyte-based agriculture: Past and present. *Annals of Botany*, *115*, 529–540. https://doi.org/10.1093/aob/mcu173

Vieira, L. R., Silva, V. N. B., Casari, R. A. D. C. N., Carmona, P. A. O., Sousa, C. A. F. D., & Souza Junior, M. T. (2020). Morpho-physiological responses of young oil palm plants to salinity stress. *Pesquisa Agropecuária Brasileira*, *55*, 1–15. https://doi.org/10.1590/s1678-3921.pab2020.v55.01835

Wang, Z., Gerstein, M., & Snyder, M. (2009). RNA-Seq: A revolutionary tool for transcriptomics. *Nature Reviews Genetics*, *10*, 57–63. https://doi.org/10.1038/nrg2484

Williams, L. J., & Abdi, H. (2010). Fisher's least significance difference test. In N. J. Salkind (Ed.), *Encyclopedia of research design* (pp. 491—494). Sage Publications. https://doi.org/10.4135/9781412961288.n154

Yan, J., Qian, L., Zhu, W., Qiu, J., Lu, Q., Wang, X., Wu, Q., Ruan, S., & Huang, Y. (2020). Integrated analysis of the transcriptome and metabolome of purple and green leaves of *Tetrastigma hemsleyanum* reveals gene expression patterns involved in anthocyanin biosynthesis. *Plos One*, *15*, e0230154. https://doi.org/10.1371/journal.pone.0230154

Zampieri, M., & Sauer, U. (2017). Metabolomics-driven understanding of genotype–phenotype relations in model organisms. *Current Opinion in Systems Biology*, *6*, 28–36. https://doi.org/10.1016/j.coisb.2017.08.007

Zhang, G., Guo, G., Hu, X., Zhang, Y., Li, Q., Li, R., Zhuang, R., Lu, Z., He, Z., Fang, X., Chen, L., Tian, W., Tao, Y., Kristiansen, K., Zhang, X., Li, S., Yang, H., Wang, J., & Wang, J. (2010). Deep RNA sequencing at single base-pair resolution reveals high complexity of the rice transcriptome. *Genome Research*, *20*, 646–654. https://doi.org/10.1101/gr.100677.109

Zhao, C., Zhang, H., Song, C., Zhu, J.-K., & Shabala, S. (2020). Mechanisms of plant responses and adaptation to soil salinity. *The Innovation*, *1*, 1–41, https://doi.org/10.1016/j.xinn.2020.100017

Zhu, H., Li, C., & Gao, C. (2020). Applications of CRISPR-Cas in agriculture and plant biotechnology. *Nature Reviews Molecular Cell Biology*, *21*, 661–677. https://doi.org/10.1038/s41580-020-00288-9

SUPPORTING INFORMATION

Additional supporting information may be found in the online version of the article at the publisher's website.

How to cite this article: Carvalho da Silva, T. L., Belo Silva, V. N., Braga, Í. de O., Rodrigues Neto, J. C., Leão, A. P., Ribeiro, J. A. de A., Valadares, L. F., Abdelnur, P. V., de Sousa, C. A. Ferreira, & Souza, M. T., Jr. Integration of metabolomics and transcriptomics data to further characterize *Gliricidia sepium* (Jacq.) Kunth. under high salinity stress. *Plant Genome*. 2021; e20182. https://doi.org/10.1002/tpg2.20182